European Journal of Medicinal Chemistry 192 (2020) 112191

Contents lists available at ScienceDirect

European Journal of Medicinal Chemistry

journal homepage: http://www.elsevier.com/locate/ejmech

Research paper

Development of bivalent triarylalkene- and cyclofenil-derived dual estrogen receptor antagonists and downregulators

Alexandra Knox [a, 1], Christina Kalchschmid [a, 1], Daniela Schuster [a, b], Francesca Gaggia [a], Claudia Manzl [c], Daniel Baecker [a], Ronald Gust [a, *]

[a] Department of Pharmaceutical Chemistry, Institute of Pharmacy, Center for Molecular Biosciences Innsbruck, University of Innsbruck, CCB – Centrum for Chemistry and Biomedicine, Innsbruck, Austria
[b] Department of Pharmaceutical and Medicinal Chemistry, Institute of Pharmacy, Paracelsus Medical University, Salzburg, Austria
[c] Institute for Pathology, Neuropathology and Molecular Pathology, Medical University Innsbruck, Innsbruck, Austria

ARTICLE INFO

Article history:
Received 9 December 2019
Received in revised form
24 February 2020
Accepted 25 February 2020
Available online 28 February 2020

Keywords:
Estrogen receptor
Dual binding mode
Homodimeric ligands
SERDs
Coactivator binding site

ABSTRACT

Up to 80% of mammary carcinoma initially exhibit estrogen-dependent growth, which can be treated by aromatase inhibitors or SERMs/SERDs. To increase the options after failure of the hormonal therapy with these drugs, the search for alternatives with a different mode of action to prevent estrogen action is of high relevance. Therefore, this study focused on the inhibition of coactivator recruitment at the estrogen receptor (ER) by targeted attachment of bivalent compounds at the coactivator binding site besides the primary binding at the ligand binding domain. Eight homodimeric 4-[1-(4-hydroxyphenyl)-2-phenyl-1-butenyl]cinnamic acid (GW7604)- or cyclofenilacrylic acid-based ER ligands with diaminoalkane linkers (C2–C5) were synthesized and their effects on the ER subtypes were assessed *in vitro*. All compounds possessed full antagonistic potency at ERα/β as determined in a transactivation assay. Furthermore, they exerted medium downregulatory effects dependent on the spacer length and did not stimulate the ER expression as observed for 4-hydroxytamoxifen. The cyclofenil-derived dimer with C4 spacer (**15b**) showed the highest binding affinity to ERα (RBA = 79.2%) and downregulated the ER content in MCF-7 cells with an efficiency of 38% at 1 μM.

1. Introduction

Regulation of estrogen receptor (ER) activity upon drug binding can be achieved *via* different ways. So far, the ligand binding site (LBS) within the ligand binding domain (LBD) is predominantly chosen as target for ER agonists or antagonists. The LBS also serves as a target for selective ER modulators (SERMs) such as tamoxifen and its active metabolite 4-hydroxytamoxifen (4-OHT, Fig. 1) [1,2].

A new approach to inhibit ER activity based on small molecules interacting with the coactivator binding site (CABS) became more important in medical chemistry in the last years [3,4]. The main challenge of this strategy, however, is the relatively low binding affinity of such compounds to the CABS owing to its size and the low number of relevant anchors [5].

Another strategy inactivating ER-mediated signal transduction was the bridging of ER dimers with bivalent compounds as a consequence of simultaneous attachment at both LBSs [6–8]. This binding mode should stabilize the dimer and effectively prevent the formation of the activation function 2 (AF2).

In a collaboration network [9,10], we designed homodimers of LBS binders (raloxifen, diethylstilbestrol and 4-OHT, respectively) with spacers of various lengths. The highest binding affinity to the ER was determined for bivalent 4-OHT compounds with spacers of approximately 22–28 Å length, allowing the proposed attachment. Interestingly, also the derivative with a spacer length of

Abbreviations: 4-OHT, 4-hydroxytamoxifen; AF2, activation function 2; CABS, coactivator binding site; DIPEA, *N,N*-diisopropylethylamine; DMEM, Dulbecco's modified eagle medium; ER, estrogen receptor; ERE, estrogen response element; E2, estradiol; FBS, fetal bovine serum; GST, glutathione S-transferase; H, helix; HRMS, high resolution mass spectrometry; LBD, ligand binding domain; LBS, ligand binding site; PBS, phosphate-buffered saline; PyBOP, benzotriazol-1-yl-oxy-tripyrrolidinophosphonium hexafluorophosphate; PGC1, peroxisome proliferator-activated receptor gamma coactivator 1; RBA, relative binding affinity; rt, room temperature; SERD, selective ER degrader; PA-SERD, pure antiestrogen and selective ER degrader; SERM, selective ER modulator; TFA, trifluoroacetic acid; TR-FRET, time-resolved fluorescence resonance energy transfer.

* Corresponding author.
E-mail address: ronald.gust@uibk.ac.at (R. Gust).
[1] These authors contributed equally to this work.

https://doi.org/10.1016/j.ejmech.2020.112191
0223-5234/

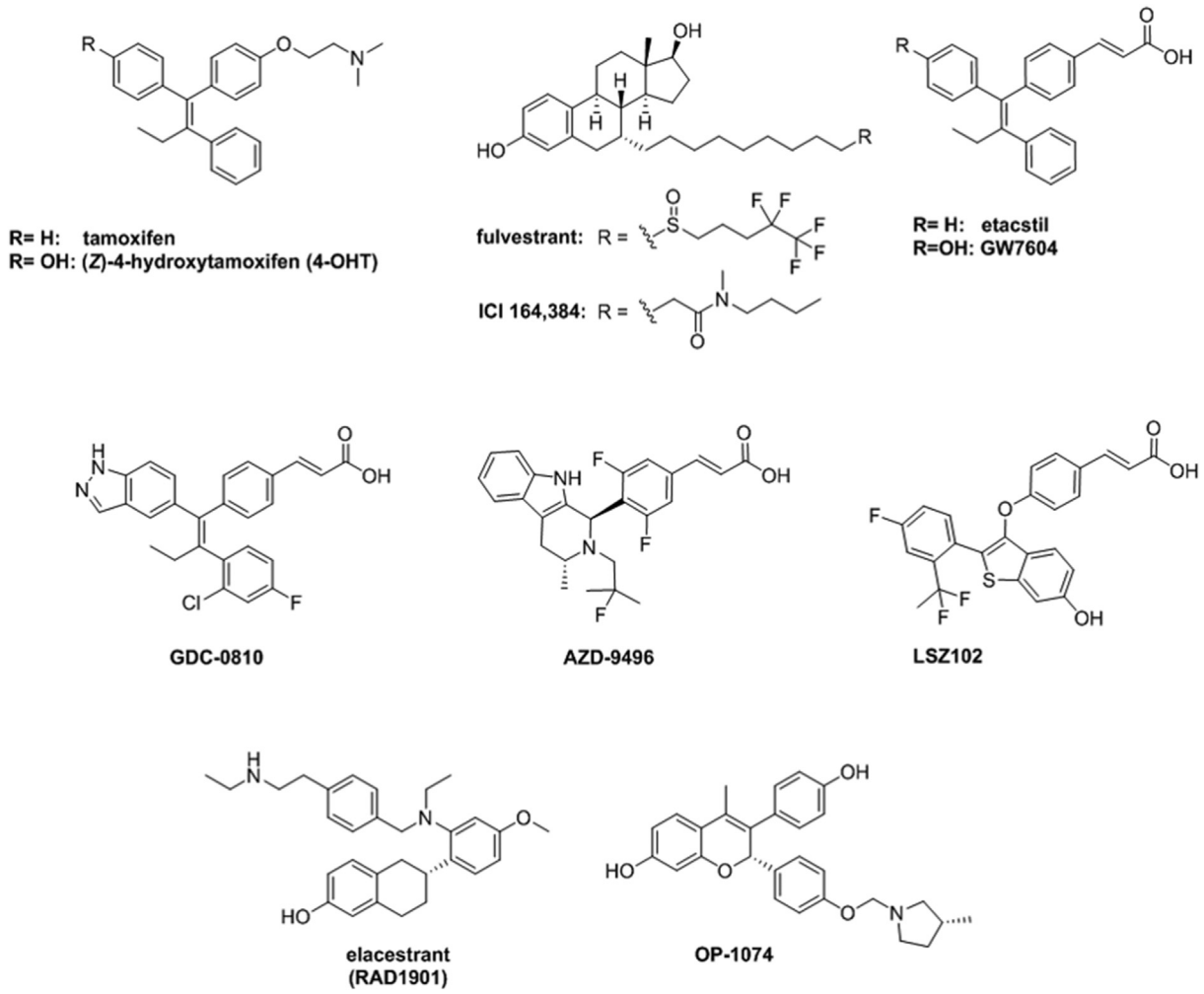

Fig. 1. Selective ER modulators (SERMs): tamoxifen and its active metabolite 4-OHT; selective ER degraders (SERDs): fulvestrant and ICI 164,384; SERM-SERDs: etacstil and its active metabolite GW7604, GDC-0810, AZD-9496, LSZ102, elacestrant (RAD1901); pure antiestrogen-SERD (PA-SERD): OP-1074.

approximately 14 Å showed high ER binding. Because the compound cannot simultaneously reach both LBSs of the ER dimer, it was assumed that it binds intramolecularly within an ER monomer with one drug moiety at the LBS and the other at the surface of the receptor. Based on theoretical studies, the interaction within the CABS as part of the binding mode was postulated. However, specific interactions were predicted. Nevertheless, this study provides a new basis for the design of bivalent drugs.

Evidence for the suitability of the CABS as a drug target, especially regarding the binding of non-peptidic small molecules, is offered by the crystal structure 2FSZ of the ERβ LBD co-crystallized with two 4-OHT molecules. One molecule of 4-OHT is bound to the LBS and the other one to the hydrophobic surface of the CABS [11]. These findings suggest that 4-OHT derivatives can generally be attached to two sites within the ER.

The crystal structure 2FSZ further allows the assumption that the unsubstituted phenyl ring deeply buried into a hydrophobic cave caused the strongest interaction of 4-OHT at the CABS [11,12]. This part of the receptor is also important for the pharmacological profile of fulvestrant. After the binding of the steroidal core to the LBS, its terminal side chain is attached to that binding groove, leading to a destabilization and consequently to a degradation of the ER in hormone-dependent cells [13]. Drugs with such a mode of action are representatives of selective ER degraders (SERDs).

For a long time, hydrophobic side chains were utilized to design estradiol (E2)-based SERDs (e.g. fulvestrant and ICI 164,384 [13,14], Fig. 1). Actually, most of the compounds used in clinical trials for the treatment of hormone-dependent breast cancer bear an acrylic acid moiety as their essential pharmacophore (e.g. GDC-0810 [15], AZD-9496 [16], and LSZ102 [17], Fig. 1). Etacstil (4-[1,2-diphenyl-1-butenyl]cinnamic acid, Fig. 1) [18] was the first acrylic acid derivative, which functions as an orally active tamoxifen-like SERM with the ability to cause degradation of the ER in hormone-dependent cells. Therefore, it was assigned as SERM-SERD.

Etacstil and its metabolite GW7604 [19,20] (Fig. 1) bind to ERα similar to 4-OHT. The acryl side chain is located in the β-channel and the carboxyl group is H-bound to Asp351 inducing a conformational shift of helix 12 (H12) to the CABS. Its location is slightly different from the one caused by 4-OHT and therefore expands the exposed hydrophobic surface of H12. The latter is made responsible for the destabilization of ERα in MCF-7 cells. The SERM activity still remains [18].

Fanning et al. identified OP-1074 as another interesting compound (Fig. 1). They declared it as a pure antiestrogen and selective ER degrader (PA-SERD), which was active in tamoxifen-resistant xenograft models [21].

Inspired by the above mentioned findings, we decided to study the consequences of simultaneously addressing the LBS and the

CABS on receptor binding and regulatory processes. Therefore, the intramolecular targeting at one ER monomer instead of intermolecular binding performed previously was the aim.

GW7604 as active metabolite of etacstil was chosen as lead structure. Compared to 4-OHT, it shows no uterotropic (agonistic) activity and is able to decrease ER levels as mentioned above. Furthermore, the triarylalkene core allows the binding to both, the LBD and the CABS, analogously to the two 4-OHT molecules offered by the crystal structure 2FSZ. The two molecules can easily be connected *via* amide bonding using various diaminoalkane spacers (**13a**-**16a**). This design allows the adjustment of the optimal distance to achieve intramolecular binding.

A disadvantage of GW7604 is the *E/Z*-isomerization at its stilbene core. The use of (E/Z)-GW7604 results in a mixture of three isomers (*EE*, *EZ*, and *ZZ*). The formation of isomers can be avoided, if a (cyclohexylidenemethylene)dibenzene core, well known from the SERM cyclofenil, is used [22,23]. Therefore, two molecules of the cyclofenilacrylic acid [22] were also connected to bivalent compounds (**13b**–**16b**).

To study the relevance of the CABS binding on the biological activity, the 1,2-diaminoethane spacer was only bound to one GW7604 molecule and the resulting monomer (**18**) was included in this study, too. Similar derivatives of ER antagonists with an acrylamide side chain have been investigated recently [23].

The impact of GW7604- and cyclofenil-based homodimer binding to the LBD on the pharmacological profile was assessed *in vitro* and the dependence of the activity on the employed spacer length was elucidated.

2. Results and discussion

2.1. Docking studies

Two molecules of GW7604 or its cyclofenilacrylic acid derivative were connected *via* amide formation with diaminoalkane spacers of various lengths. These spacers mediated a sufficient hydrophobicity for the interaction with the coactivator binding area and allowed high flexibility for the attachment at both binding sites.

To estimate the optimum distance of the terminal drugs to achieve high binding affinity, theoretical studies were performed (for details see Experimental section). Chains ranging from C2 to C8 were chosen for both series and docking results were compared. Due to the known binding properties of 4-OHT within the CABS, the crystal structure 2FSZ of ERβ was used. ERα and ERβ are highly conserved in their LBD. The ligand binding sites differ only in two amino acids: Leu384 and Met421 in ERα are replaced by Met336 and Ile373 in ERβ, respectively [12,24].

It is noteworthy that the following theoretical considerations are discussed based on the *EE* isomer, because in this case the two biologically relevant (*E*)-GW7604 molecules are connected. Furthermore, calculations with the respective *EZ* and *ZZ* isomers pointed to an inferior binding to the LBS and CABS.

After the attachment to the LBS, the terminal drug cannot adapt a pose comparable to 4-OHT at the CABS. In each case, it docks in a flipped orientation with the acrylate moiety, which is directed to the LBS, and the ethyl group which is located outside the receptor binding pocket (Fig. 2A and B). Nevertheless, various cavities at the CABS can be targeted.

When employing a C2 spacer, the phenyl ring of **13a** (formula, Fig. 3) is partially buried into the same groove at the CABS as 4-OHT in 2FSZ, while the spacer is surrounded by Leu306, Met309, Ile310, Leu331, and Trp335 forming exclusively lipophilic contacts, comparable to the side chain of ICI 164,384. Elongation of the spacer leads to a more relaxed conformation: compound **14a** (C3 spacer, Fig. 3) forms an additional H-bond from the phenolic OH to Gln327 (Fig. 2A). This amino acid has previously been described as crucial for binding small molecules to the CABS [3]. The C5 derivative **16a** (Fig. 3) also shows an H-bond with the charge clamp residue Lys314 (Fig. 2C), while further elongation of the aliphatic chain disturbs the accommodation of the terminal scaffold at the CABS.

These theoretical investigations indicate that two different subpockets at the CABS could be utilized by bivalent drugs. One cavity is located 9–10 Å away from the nitrogen of the GW7604-amide bound to the LBS and is addressed mainly by hydrophobic contacts with residues of helices H3–H5. The second, clearly more hydrophilic binding surface, is located 18–20 Å from the LBS. Gln327 and charge clamp residue Lys314 constitute anchoring points for hydrophilic residues. An intermolecular binding mode is rather unlikely, as it would require a linker length of 22 Å [10].

The C2 spacer of the cyclofenil-based homodimer **13b** (Fig. 3) seems to be too short to reach the hydrophobic groove or mediate relevant H-bonding to the CABS. However, **13b** could adapt an agonistic binding mode as found for an E2 derivative in the crystal structure 2YAT [25]. It describes the ERα LBD co-crystallized with E2 that is linked to a metal chelate. The E2 moiety is bound to the LBS and the side chain (metal chelate) protrudes from the LBS towards H7 and not H12 and therefore the agonistic potency is retained. In our theoretical studies, only **13b** was able to bind in this manner.

The amino acid Gln327 located in the second binding surface seems to contribute significantly to the interactions of the cyclofenil-based homodimers at the CABS. Unlike the GW7604-based dimers, this region is not reached with a C3 (**14b**, Fig. 3), but only with a C5 spacer (**16b**, Fig. 3) that allows the formation of an H-bond from the terminal cyclofenil to Gln327, being close enough to charge clamp residue Lys314 (Fig. 2D). Additionally, hydrophobic contacts within the lipophilic surface are possible as well.

2.2. Chemistry

Based on the above-mentioned theoretical studies, two molecules of GW7604 or the cyclofenilacrylic acid were linked by C2 to C5 spacers, respectively. For the synthesis of the precursors, a procedure frequently used for stilbene derivatives was used, which has partly been described for GW7604 as well (Scheme 1) [26–29].

The synthesis is comprised of a Friedel-Crafts acylation of acyl chloride **7a** with anisole (method a) followed by a Grignard coupling with Mg/4-bromobenzaldehyde diethyl acetal and a dehydration step (method b), which led to a mixture of *E/Z* isomers [27]. The stereo-selective Wittig-Horner reaction enabled the introduction of an isomerically pure *E*-acrylate side chain (method c; compound **10a**). Ester hydrolysis (method d) and ether cleavage (method e) yielded 4-[(*E/Z*)-1-(4-hydroxyphenyl)-2-phenyl-1-butenyl]cinnamic acid (GW7604 = **12a**). The cyclofenilacrylic acid **12b** was analogously synthesized (Scheme 1, methods a-e).

Subsequently, two acrylic acid moieties (**12a** or **12b**) were connected *via* diamide formation (method f). The phosphonium salt based coupling reagent PyBOP [30] was chosen for this reaction, having the advantage of combining high yields with an easy handling. The dimerization to compounds **13a,b-16a,b** is depended on the temperature, the solubility of the final product, and the applied chain length.

Finally, the GW7604 derivative **18**, having only an 1,2-diaminoethane side chain, was synthesized upon amide coupling of **12a** with *N*-Boc-1,2-diaminoethane (→ compound **17**) followed by Boc cleavage with TFA and an isolation as trifluoroacetate salt (**18**, Scheme 2).

All compounds were characterized by ^{1}H and ^{13}C NMR spectroscopy as well as high resolution mass spectrometry (HRMS) and

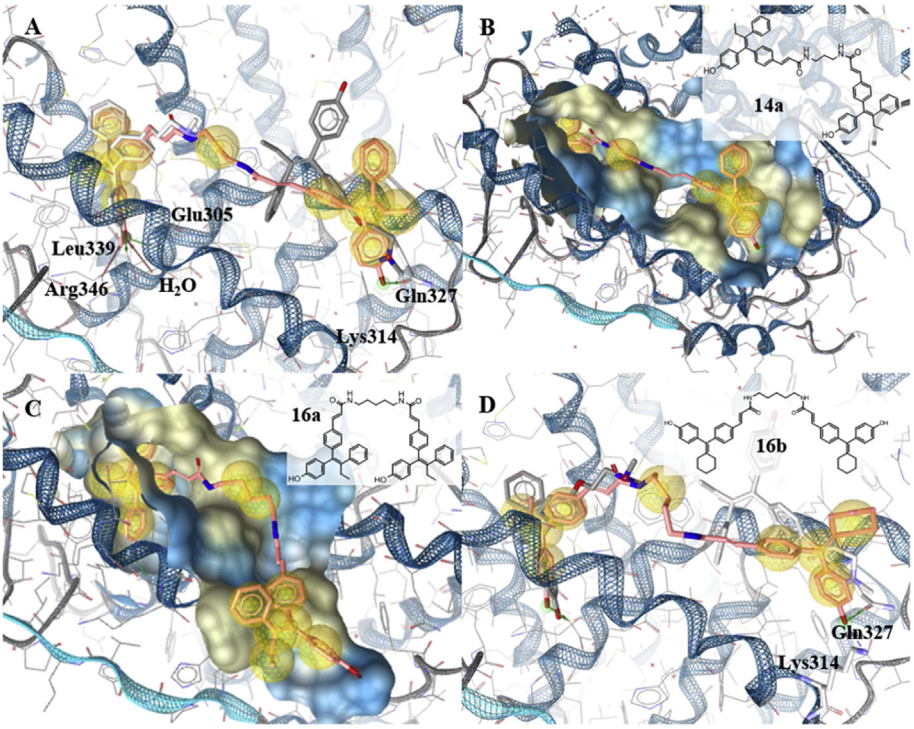

Fig. 2. ERβ LBD of 2FSZ co-crystallized with two 4-OHT molecules (depicted in grey) and docked ligands (depicted in rose). Hydrophobic protein-ligand contacts are indicated by yellow spheres, H-bonds by red and green arrows. (**A**) Compound **14a**: The moiety occupying the LBS forms H-bonds with Arg346, Glu305, and a water molecule in a classic manner and in this case additionally with Leu339. In the CABS an H-bond to Gln327 is formed. The receptor binding pocket with homodimer **14a** (**B**) and **16a** (**C**): Hydrophobic contacts are indicated in yellow, hydrophilic interactions in blue. (**D**) Docked cyclofenil-based homodimer **16b**: Charge clamp residue Lys314 is shown in the foreground; Gln327 forms an H-bond with the phenolic group of the cyclofenil derivative occluding the CABS. (For interpretation of the references to color in this figure legend, the reader is referred to the Web version of this article.)

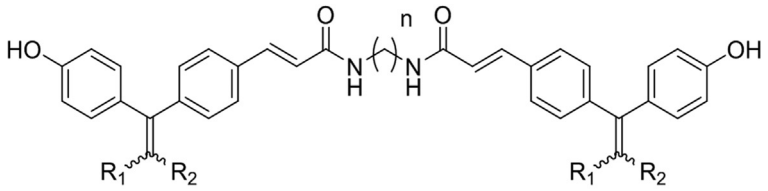

compound	R_1	R_2	n
13a		CH_2CH_3	2
14a			3
16a			5

compound	R_1	R_2	n
13b			2
14b			3
16b			5

Fig. 3. GW7604- and cyclofenil-based homodimers **13a,b**, **14a,b**, and **16a,b**.

HPLC analyses. The purity was >95% in each case. However, the compounds **13a**-**16a** are a mixture of isomers (*EE*, *EZ*, *ZZ*), because GW7604 used in the synthesis was not isomerically pure (see above). The NMR spectra showed signals, which were assigned to the isomers by 2D NMR (see Supplementary data).

Using the example of **14a**, an isomer ratio of EE:EZ:ZZ = 25:50:25 was found and remained constant throughout three days of incubation in MeOH/2x PBS at 37 °C (see Experimental section and Supplementary data), similar to the findings on 4-OHT-derived homodimers reported by Shan et al. [10].

Isomerization of a 4-hydroxystilbene or triarylalkene core during the synthesis is a general problem in this class of compounds [31,32]. Classical synthesis routes leading to GW7604 other than that used in this study, e.g. McMurry and Heck-coupling reactions [22], cannot improve the *E*/*Z* ratio and were found to have less total yield as well as difficulties in scaling up.

However, it should be mentioned that it is possible to separate (*E*)-GW7604 from the mixture by crystallization, but geometric isomerism occurs immediately in solution as already determined for 4-OHT. (*Z*)-4-OHT undergoes 20–30% isomerism after

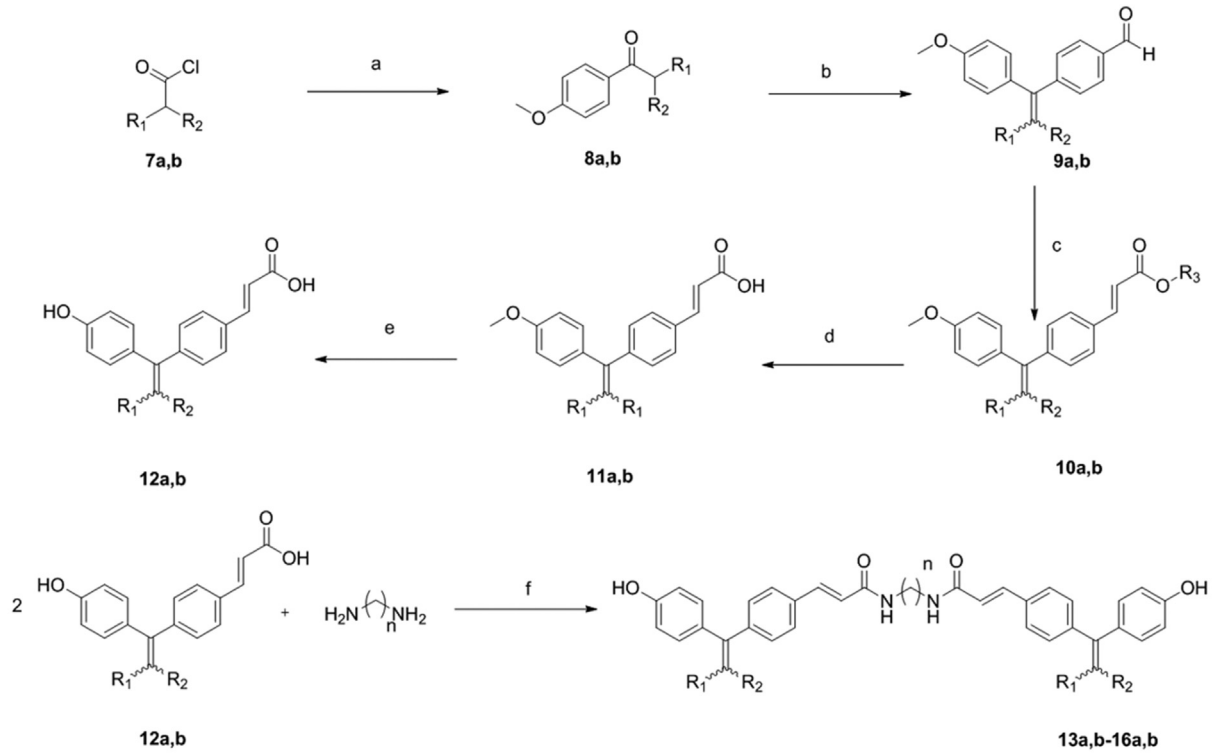

compound	R_1	R_2	R_3	n
7a-9a, 11a, 12a		CH_2CH_3	-	-
10a			CH_2CH_3	-
13a			-	2
14a			-	3
15a			-	4
16a			-	5

compound	R_1	R_2	R_3	n
7b-9b, 11b, 12b				
10b			CH_3	-
13b			-	2
14b			-	3
15b			-	4
16b			-	5

Scheme 1. Synthesis pathway of compounds **12a,b** and **13a,b-16a,b:** Reagents and conditions: (a) anisole, $AlCl_3$, anh. DCM, 0 °C to room temperature (rt), 2.5 h (yields: 61–76%); (b) i) Mg, 4-bromobenzaldehyde diethyl acetal, anh. THF, rt, 4 h; ii) EtOH, HCl conc., reflux, 5 h (yields: 63–73%); (c) trimethyl-/triethylphosphonoacetate, potassium bis(trimethylsilyl) amide, anh. THF, 0 to −78 °C to rt, 20 h (yields: 76–85%); (d) THF:EtOH = 1:1, 2N KOH, rt, 24 h (yields: 85–99%); (e) BBr_3, anh. DCM, 0 °C, 2 h (yields: 66–92%); (f) DIPEA, PyBOP, anh. DMF, anh. DCM, 0 °C to rt to 45 °C, 20 h to 3 d (yields: 28–75%).

incubation for two days in cell-free culture medium at 37 °C and also in ethanol stock solutions at −20 °C [32,33]. Experiments that lasted up to six months showed an equilibrium of *E*:*Z* = 50:50, regardless of the applied conditions [34].

GW7604 is mostly investigated as an *E*/*Z* mixture [23,35], but it was reported that the effects at the isolated ER [22] as well as in cell-based assays can be assigned to the more active *E* isomer [35]. It is noteworthy that the bivalent cyclofenil derivatives are isomerically pure.

2.3. Biological evaluation

2.3.1. Ligand binding affinity

The binding affinities of the GW7604- or cyclofenil-based homodimers to the LBS, expressed as relative binding affinity (RBA) compared to E2 (100%), were assessed in a TR-FRET assay on the isolated human ERα/ERβ LBDs. 4-OHT, GW7604, and fulvestrant were used as references.

4-OHT showed an RBA value of 14.7% for ERα and 60.7% for ERβ. The exchange of the basic side chain with an acrylic acid moiety (GW7604) reduced the affinity to 6.2% (ERα) and 27.1% (ERβ). Both compounds were 4.5-fold more selective for ERβ (Table 1).

Derivatization of GW7604 with an 1,2-diaminoethane chain (→ **18**) reduced the binding to ERα further (RBA = 2.6%), while that to ERβ remained unchanged (RBA = 23.9%). Interestingly, an additional GW7604 moiety at **18** resulting in the bivalent compound **13a** did not influence the binding to ERα (RBA = 2.2%), but strongly reduced the interaction with ERβ (RBA = 1.5%).

The elongation of the spacer by one (→ **14a**) or three methylene groups (→ **16a**) increased the RBA to ERα (25.9% or 9.4%,

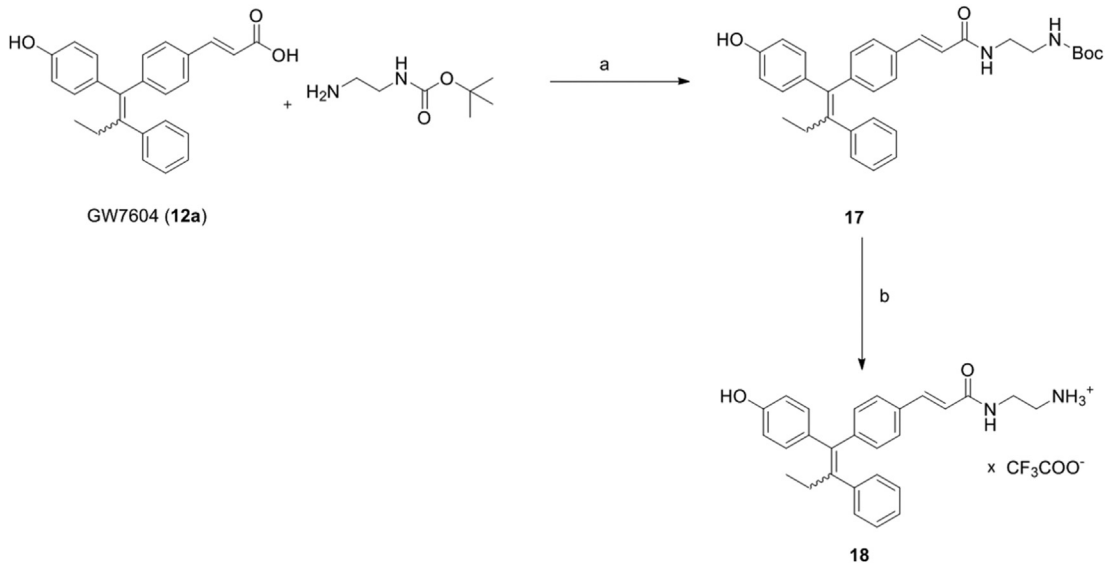

Scheme 2. Synthesis of monomer **18**.
Reagents: (a) DIPEA, PyBOP, anh. DMF, anh. DCM, rt, 24 h (yield: 51%); (b)TFA, anh. DCM, 0 °C, 2 h, (quant.).

Table 1
In vitro competitive binding assay.

Compound	TR-FRET[a] ERα		RBA ERα	TR-FRET[a] ERβ		RBA ERβ
	IC_{50} [nM]		%	IC_{50} [nM]		%
13a	15.1	±5.6	2.2	67.7	±8.3	1.5
14a	1.28	±0.51	25.9	22.2	±8.8	4.6
15a	18.9	±4.0	1.9	44.0	±17.5	2.3
16a	3.52	±0.95	9.4	15.5	±9.1	6.6
13b	6.43	±2.64	5.1	27.5	±11.9	3.7
14b	1.67	±0.59	19.7	34.0	±19.8	3.0
15b	0.42	±0.10	79.2	15.7	±9.5	6.5
16b	2.35	±0.76	14.1	17.5	±2.7	5.8
18	13.6	±2.8	2.6	4.26	±0.66	23.9
4-OHT	2.24	±0.89	14.7	1.68	±1.00	60.7
GW7604	5.35	±1.39	6.2	3.77	±1.06	27.1
fulvestrant	2.85	±0.83	11.6	10.2	±2.5	10.0
E2	0.33	±0.19	100	1.02	±0.50	100

[a] Displacement of fluorescent-labeled E2 from ERα or ERβ by GW7604- or cyclofenil-based homodimers. IC_{50} values represent means ± SD of ≥ 3 independent experiments.

respectively). The C4 derivative **15a** (RBA = 1.9%) showed the same affinity as **13a**. It should be mentioned that the RBA value of **16a** was comparable to that of fulvestrant (RBA = 11.6%) and the binding affinity of **14a** was even higher than that of 4-OHT (RBA = 14.7%).

Interestingly, GW7604-derived compounds showed higher affinity to ERα compared to ERβ. The ERα/ERβ ratio based on the TR-FRET increased in the series **15a** (0.83) < **16a** (1.42) = **13a** (1.47) < **14a** (5.63) (compare RBAs at ERα and ERβ in Table 1).

In the cyclofenil-based series all compounds possessed equal (**13b**, RBA = 5.1%) or higher affinity to ERα than GW7604 (RBA = 6.2%). An extraordinary high RBA value of 79.2% was determined for **15b** (C4 derivative). This finding contradicts the molecular docking studies that proposed a stable binding pose at the CABS only for the C5 derivative **16b** (RBA = 14.1%). Compound **14b** (C3 spacer, RBA = 19.7%) showed a 3-fold higher affinity than GW7604, too.

It is noteworthy that also the cyclofenil derivatives demonstrated subtype selectivity for ERα (ERα/ERβ ratio (based on the TR-FRET)): **13b** (1.38) < **16b** (2.43) < **14b** (6.57) < **15b** (12.18).

For the interpretation of the results concerning ERα, the theoretical studies are helpful, because the TR-FRET assay studied the drug-ER interactions on the molecular level. The derivation of GW7604 (→ **18**) slightly reduced the affinity to the ER. Even the binding of a second GW7604 molecule to **18** (→ **13a**) did not influenced the RBA. The spacer is too short to reach the hydrophobic pocket at the CABS located at a distance of 9–10 Å of the LBS. This is possible if the spacer is elongated by one methylene group (C3 spacer, → **14a**). Docking analyses documented further that the optimum spacer length (C5 spacer, → **16a**) allowed H-bonding of the second GW7604 moiety of the dimer with Gln327 and Lys314, respectively, approximately 18–20 Å away from the LBS.

The RBA values of the compounds **13b**–**16b** were higher than that of the respective GW7604 dimers, which very likely results from the presence of the isomeric mixture in case of GW7604 dimers. The molecular docking studies revealed that the *EE* isomers, which constitute only 25% of the GW7604 series, possess the spatial structure necessary for the simultaneous binding to the LBS and CABS. The *EZ* (50%) and *ZZ* (25%) isomers contribute to this effect to a much smaller extent, because of an unfavorable attachment to the LBS and/or the CABS (see molecular docking).

2.3.2. Coactivator recruitment

In a further TR-FRET experiment, the influence of the compounds on the attachment of the coactivator PGC1 at the ERα LBD was investigated. E2 showed a recruitment of 100% at 10 nM (for details see Supplementary data). The bivalent compounds did not induce PGC1 binding up to a concentration of 1 μM. Interestingly, the cyclofenil derivative **13b** was also inactive, although an agonistic binding mode is generally possible according to theoretical studies (see above).

The coactivator binding was also investigated in the presence of E2 (at EC_{50} = 4 nM) by taking the examples of GW7604 as well as **14a,b** and **15a,b**.

GW7604 completely antagonized the E2 stimulating effects after an incubation time of 10 min only at concentrations higher than 1 μM. After incubation for 30 min, a maximum of about 50% of inhibition was observed at 5 μM.

The bivalent compounds were distinctly more active. All

compounds inhibited the coactivator recruitment, which is induced by E2 more than 75% at the lowest concentration of 5 nM and antagonized the E2 effect completely (100%) at 100 nM (Fig. 4). In contrast to GW7604, **14a,b** and **15a,b** were still active at 100 nM (about 50% inhibition) after an incubation for 30 min. At 1 μM, **14a** and **15a** even completely prevented coactivator binding.

These findings clearly indicate that contrary to GW7604 the E2-induced coactivator recruitment can be effectively blocked by bivalent compounds.

2.3.3. Inhibition of transactivation

To obtain further information about the influence of the compounds on the signal transduction, a cellular assay with U2OS cells transiently transfected with the ER plasmids pSG5-ERα or pSG5-ERβ and the reporter plasmid p(ERE)2-luc$^+$ as well as pRenilla-CMV for standardization was used. The expression of luciferase is a measure for binding ER dimers to the estrogen response elements (EREs) at the reporter plasmid.

None of the compounds caused agonistic effects at 0.1 μM or 1.0 μM, which confirmed the inability of coactivator recruitment (see above). Alternatively, this could also be caused by the blocking of ER dimerization upon drug binding, preventing the interaction with the reporter plasmid, too.

In contrast, all bivalent compounds proved to be potent antagonists and inhibited the transactivation of E2 at ERα (E2 conc.: 0.03 nM) and ERβ (E2 conc.: 0.3 nM), respectively. The resulting concentration-ERα activation curves are depicted in Fig. 5 and the IC_{50} values are listed in Table 2.

Interestingly, the most potent GW7604 derivative was **18** with an IC_{50} = 5.33 nM at ERα and IC_{50} = 3.62 nM at ERβ. It prevented gene activation comparable to 4-OHT (ERα: IC_{50} = 2.28 nM; ERβ: IC_{50} = 0.99 nM). Derivation of **18** to the GW7604 derivatives **13a**-**16a** reduced the antagonistic effects at ERα (IC_{50} = 136–290 nM). Compounds **14a** (IC_{50} = 136 nM) and **16a** (IC_{50} = 160 nM) were still 2-fold more active than GW7604 (IC_{50} = 238 nM). Compounds **13a** (IC_{50} = 260 nM) and **15a** (IC_{50} = 290 nM) were less effective, but reached the GW7604 potency. The inhibitory effects at ERβ were comparable to that at ERα (Table 2). Only **13a** (IC_{50} = 78.7 nM) possessed slight ERβ subtype selectivity.

Within the cyclofenil series, except for compound **14b** (ERα: IC_{50} = 565 nM; ERβ: IC_{50} = 304 nM), all compounds were more potent antagonists than their GW7604 analogues. The most efficient inhibitors were **15b** and **16b** with IC_{50} = 88.3 and 73.0 nM at ERα and IC_{50} = 54.8 and 49.4 nM at ERβ, respectively.

It is worth mentioning that fulvestrant caused an unusual concentration activity curve, completely inhibiting the E2-stimulated luciferase expression even at the lowest concentration (0.05 nM). Such an activity profile can be explained by the induction of an extraordinarily high ER downregulation (see below). The calculation of its IC_{50} values was not feasible.

2.3.4. Estrogen receptor downregulation

Next, the influence of the compounds on the ERα content in MCF-7 cells was studied. The ERα expression after 24 h of incubation with the respective compound (1 μM) was analyzed by Western blotting. β-actin was used as loading control (Fig. 6). Additionally, the receptor protein was quantified by In-Cell Western analyses (Table 3).

The treatment of the MCF-7 cells with the SERD fulvestrant for 24 h led to an almost complete degradation of ERα. Tamoxifen and especially its active metabolite 4-OHT are SERMs with a mixed agonistic/antagonistic pharmacological profile and stabilize the receptor [36,37]. Therefore, 4-OHT strongly increased the protein level, as visible in the Western blot (Fig. 6).

The comparison of the blots obtained for 4-OHT and GW7604 demonstrates the relevance of the side chain for interference with ERα expression. In contrast to 4-OHT (dimethylaminoethanol side chain), GW7604, which has an acrylic acid moiety, caused slight degradation. The GW7604 derivative **18** increased the ERα content in the cells. The stimulating properties depended on the presence of a free, under physiological conditions cationic side chain. The binding of a second GW7604 molecule to **18** resulted in the uncharged bivalent compound **13a** with low degradation potency. The latter was increased by an elongation of the spacer (→ **14a**-**16a**). The same trend was observed for the cyclofenil derivatives **13b**–**16b**.

Based on the Western blot analyses, the bivalent compounds induced ERα degradation without carrying an acrylic acid side chain. Therefore, it was of interest to quantify the cytosolic receptor in an In-Cell Western immunoassay (Table 3).

As expected, at a concentration of 1 μM only 4-OHT and **18** upregulated the ERα protein level compared to the DMSO control (100%) to 263% and 165%, respectively. The efficacy of **13a** was low (11%), but was enhanced by elongation of the spacer length. **14a** caused the highest ER downregulation to 51% (efficacy: 49%) compared to the control, **15a** (efficacy: 32%) and **16a** (efficacy: 36%) were slightly less active. The same trend was observed in the cyclofenil-based series. The most active compound was **14b** (efficacy: 51%) followed by **15b** (efficacy: 38%), **16b** (efficacy: 21%), and **13b** (efficacy: 8%).

Compared to fulvestrant (efficacy: 100%), the compounds were SERDs of moderate potency (Fig. 7), whereby only **14a** and **14b** reached downregulation of 50% and were basically as efficient as GW7604 (efficacy: 56%).

In conclusion, cationic compounds such as 4-OHT or **18** showed SERM-like activity. Although they antagonized the E2 effects in the

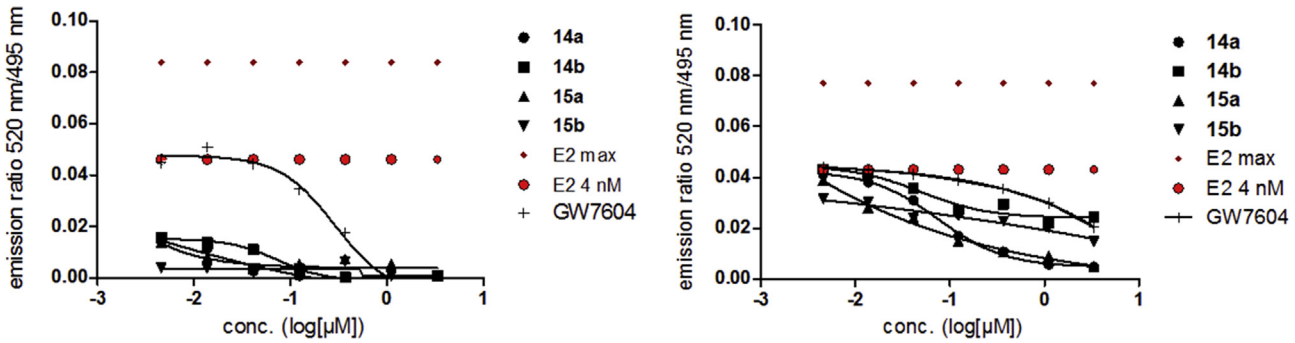

Fig. 4. Inhibition of coactivator recruitment by concomitant administration of bivalent compounds **14a,b** and **15a,b** with E2 (4 nM). Incubation time: 10 min (left) and 30 min (right).

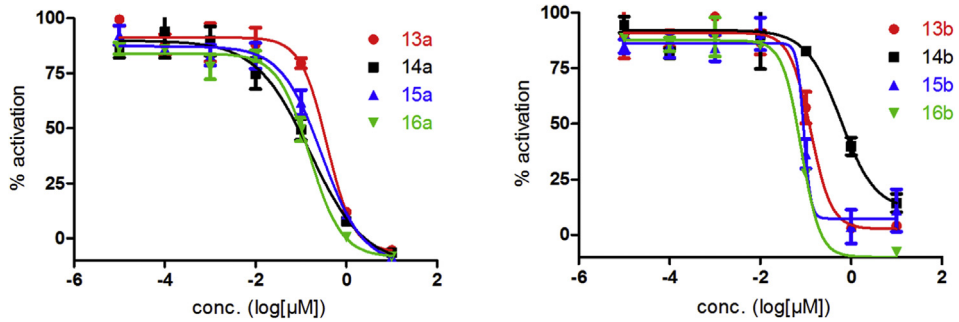

Fig. 5. Inhibition of ERα transactivation in U2OS cells transiently transfected with the ER plasmids pSG5-ERα and p(ERE)2-luc^{+}. GW7604-based homodimers (left) and cyclofenil-based homodimers (right).

Table 2
Luciferase reporter gene assay (ERα and ERβ) using U2OS cells, transiently transfected with plasmids pSG5-ERα or pSG5-ERβ and the reporter plasmid p(ERE)2-luc^{+}.

Compound	Transactivation ERα IC_{50}[a] [nM]		Transactivation ERβ IC_{50}[a] [nM]	
13a	260	±70	78.7	±9.4
14a	136	±28	153	±53
15a	290	±57	215	±155
16a	160	±52	256	±112
13b	131	±14	216	±135
14b	565	±43	304	±160
15b	88.3	±2.3	54.8	±28.8
16b	73.0	±6.4	49.4	±33.1
18	5.33	±3.23	3.62	±1.43
4-OHT	2.28	±1.34	0.99	±1.25
GW7604	238	±74	154	±53
fulvestrant	n.d.[b]		n.d.[b]	

[a] IC_{50} values represent means ± SD of ≥3 independent experiments.
[b] n.d.: not defined.

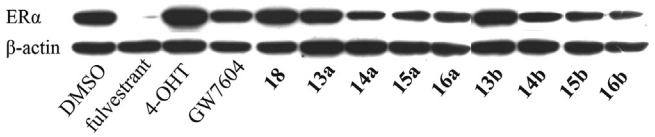

Fig. 6. ERα expression levels in MCF-7 cells after incubation with the compounds (1 μM) for 24 h.

luciferase reporter gene assay (Table 2), they stimulated ERα expression in MCF-7 cells. In contrast, GW7604 and its dimers as well as the cyclofenil analogues were SERDs of medium potency. The most active compounds **14a** and **14b** showed high binding affinity to ERα and were pure antagonists in the transactivation assay and can be assigned to the group of PA-SERDs. The biological activity depended on the spacer length, which indicates a selective

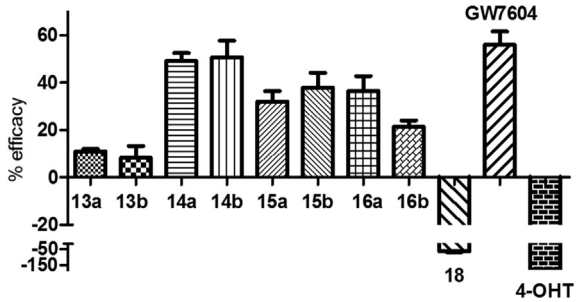

Fig. 7. Percent efficacy related to fulvestrant. Compound **18** and 4-OHT showed upregulation. Values represent means + SD of ≥3 independent experiments.

interaction with the target molecule, the ER.

Generally, the reduced intracellular ERα content can be seen as the consequence of a lower expression or an increased degradation of the receptor protein. Therefore, the influence of the ubiquitin-proteasome pathway [38] on the degradation was studied on the examples **14a**, GW7604 and fulvestrant. The cells were incubated with the respective compound (1 μM) either with or without the proteasome inhibitor MG-132 (1 μM) [39]. The receptor protein content was analyzed by Western blotting.

As depicted in Fig. 8, MG-132 marginally blocked the effects of fulvestrant and GW7604. The degradation caused by **14a** was unaffected by MG-132, which indicates that the reduced ERα content is not caused by the ubiquitin-proteasome pathway.

It is well known that the ER enters the proteolytic pathways through alternate mechanisms depending on the ligand-induced structure modifications. In the case of fulvestrant and GW7604, distinct effects on the compartmentalization of the ERα within the cell have been revealed. The E2-induced receptor shape enables the recognition of the proteasome and the subsequent degradation.

Table 3
ERα levels in MCF-7 cells determined by In-Cell Western immunoassay.

Compound	% ERα Remaining[a]	% Efficacy[b]	Compound	% ERα Remaining[a]	% Efficacy[b]
13a	89.0 ± 1.6	11	**13b**	91.8 ± 5.6	8
14a	50.6 ± 4.6	49	**14b**	49.1 ± 6.7	51
15a	68.0 ± 5.1	32	**15b**	62.0 ± 7.4	38
16a	63.9 ± 3.1	36	**16b**	78.5 ± 9.2	21
18	165.0 ± 4.0	[c]	fulvestrant	0	100
GW7604	44.3 ± 12.1	56	DMSO	100	0
4-OHT	263.0 ± 9.0	[c]			

[a] ERα levels compared to solvent control (DMSO). Values represent the mean of ≥3 independent experiments ± SD.
[b] Efficacy at 1 μM, calculated as downregulation of ERα compared to the efficacy of reference compound fulvestrant.
[c] Upregulation.

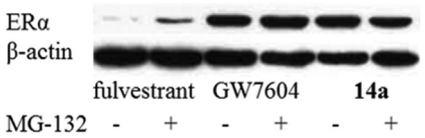

Fig. 8. ERα expression levels in MCF-7 cells after 4 h of incubation with 1 μM of the compounds, either with or without the protease inhibitor MG-132 (1 μM).

2.3.5. Solubility and cellular uptake

Essential parameters for the interpretation of cellular effects are the water solubility and the cellular uptake of drugs.

Compounds which are part of the GW7604 series showed higher solubility in aqueous solutions (**13a**: >40 μM; **14a**: 24 μM; **15a**: 19 μM; **16a**: 34 μM) than fulvestrant (11.1 μM). Cyclofenil derivatives are more lipophilic, which hampers the dissolution in water (saturation concentration: **13b**: 6.5 μM; **14b**: 15.4 μM; **15b**: 10 μM; **16b**: 10 μM). In all cases, however, it was possible to reach the concentrations necessary for the above described cell culture experiments.

Uptake studies (at 10 μM, 24 h of incubation) were performed on the examples **18**, **15a**, and **15b**, based on the inherent fluorescence of their cinnamide scaffold.

All compounds were taken up in ER-positive MCF-7 cells (Table 4), **15a** and **15b** to the same amount of about 5 nmol/mg protein. Interestingly, the positive charge of **18** enabled an approximately 7-fold enrichment (35.3 nmol/mg protein) compared to the other compounds. Because **15a** and **18** caused comparable intracellular amounts in MCF-7 and the fibroblast-like COS-7 cells (about 4 and 34 nmol/mg protein, respectively), it is very likely that the uptake is not receptor mediated. The content of **15b** was even higher in COS-7 cells (11.7 nmol/mg protein). The parent compound GW7604 did not provide adequate relative fluorescence intensity and therefore could not be used as reference for the cellular uptake studies.

2.3.6. Antiproliferative effects

The influence of the bivalent drugs on the growth of hormone-dependent, ER-positive MCF-7 breast cancer cells was investigated in a standardized crystal violet assay. For this purpose, the cells were incubated with compounds for 72 h and the cell mass was quantified by staining and measuring the absorbance [40]. The reduction of cell mass correlates with the antiproliferative effects of the drugs.

GW7604 as a reference caused a very flat concentration-activity curve and reached a T/C value of 75.5% at 10 μM. Therefore, it was not feasible to calculate the IC_{50} value from this curve (Fig. 9). The cellular behavior differs from that described in the literature where IC_{50} values up to 2 μM are described [41]. This discrepancy might be the consequence of different conditions used in the assays, e.g. the number of cells seeded and the incubation time. For instance, Fan et al. determined a greater distance between test and control curves for GW7604 only with increased incubation time. After 72 h the differences of antiproliferative effects were marginal [27].

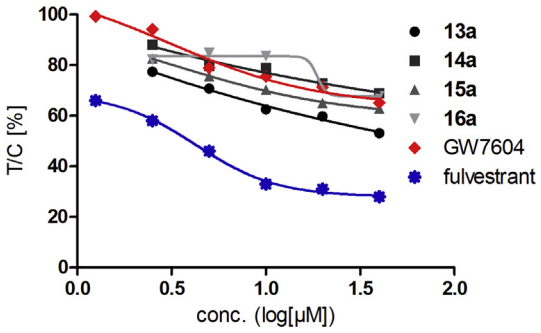

Fig. 9. Antiproliferative effects on MCF-7 breast cancer cells, determined in the crystal violet assay. T is the biomass of cells treated with compounds for 72 h; C is the biomass of control cells after 72 h.

The curve of fulvestrant is flat as well, but started with lower T/C values (T/C = 64% at 50 nM) and reached T/C = 33% at 10 μM, which allowed the calculation of IC_{50} = 4.93 μM.

All bivalent compounds showed concentration-activity curves similar to GW7604, which does not allow a reasonable calculation of the IC_{50} values. The use of higher concentrations was restricted by the insufficient solubility above 20 μM. The reduced cell mass at 10 μM (see Table 1 in Supplementary data) generally documented antiproliferative effects. Analogous results were achieved with the cyclofenil derivatives, whereby lower water solubility allowed compound concentrations only up to 10 μM.

Interestingly, compound **18** caused the expected sigmoid concentration-activity curve, from which an IC_{50} = 4.95 μM (Table 5) was calculated. Thereby, **18** was as active as 4-OHT (IC_{50} = 4.94 μM). The antiproliferative effects of both compounds were not restricted to MCF-7 cells. They also reduced the growth of ER-negative, non-tumorous COS-7 cells (**18**: IC_{50} = 5.95 μM; 4-OHT: IC_{50} = 8.69 μM). Such unspecific effects are well known for 4-OHT and are associated with cancerogenic DNA adducts determined for instance in hepatocytes [42] and the endometrium [43]. In contrast, fulvestrant was 7-fold more effective against MCF-7 cells (IC_{50} = 4.93 μM) compared to COS-7 cells (IC_{50} = 34.0 μM).

The antiproliferative effects were further evaluated against MDA-MB-231 and SKBr-3 breast cancer cells. The bivalent derivatives were inactive at the concentration used (see Supplementary data). In contrast, 4-OHT as reference reduced the cell mass at 10 μM as well as 20 μM independent of the cell line used. It inhibited the proliferation at 10 μM to 79% (MDA-MB-231) and 58% (SKBr-3), respectively. At 20 μM even cytocidal effects were observed (MDA-MB-231: T/C = −80%; SKBr-3: T/C = −81%). These findings confirmed the ER-independent influence of 4-OHT on the cell growth. They are further an indication that the bivalent compounds exert their biological activity mainly due to the interaction with ERα. MDA-MB-231 cells are ERα-negative and ERβ-positive, while SKBr-3 are negative concerning both subtypes (ERα-negative, ERβ-negative).

Table 4
Cellular uptake of compounds **15a**, **15b**, and **18** (10 μM) after 24 h of incubation.

Compound	MCF-7 cells [nmol compound/mg protein][a]		COS-7 cells [nmol compound/mg protein][a]	
15a	4.67	±1.28	3.92	±0.49
15b	5.22	±1.68	11.7	±0.8
18	35.3	±7.0	33.7	±7.8

[a] Values represent means ± SD of ≥3 independent experiments.

Table 5
Antiproliferative effects against ER-positive MCF-7 and the fibroblast-like COS-7 cells.

Compound	MCF-7		COS-7	
	IC_{50} [μM][a]		IC_{50} [μM][a]	
18	4.95	±1.43	5.95	±1.03
4-OHT	4.94	±0.26	8.69	±1.20
fulvestrant	4.93	±1.06	34.0	±4.1

[a] Values represent means ± SD of ≥3 independent experiments.

2.3.7. Antimetabolic activity

In addition to the antiproliferative effects, the antimetabolic activity of the compounds was quantified in a modified MTT assay (EZ4U). The mitochondrial guided transformation of a tetrazolium salt to its colored formazan is a tracer for cell viability. The compounds were tested for activity on the MCF-7 and COS-7 cell lines (Fig. 10). Regarding their low water solubility, cyclofenilacrylic acid derivatives **13b**–**16b** and GW7604 were tested only up to a concentration of 10 μM.

The results obtained from the modified MTT assay partially differed from that of the crystal violet assay. GW7604 was completely inactive towards MCF-7 cells at the used concentrations. Among the GW7604 derivatives, **13a** and **15a** reduced the metabolic activity to 45% and 70% at 20 μM. The cyclofenil derivatives **14b**, **15b**, and **16b** showed a reduction to 53%, 69%, and 50% at 10 μM, respectively. Interestingly, compound **18** (60% at 20 μM) was less active than 4-OHT (18% at 20 μM), but showed similar effects to fulvestrant (61% at 20 μM).

None of the homodimeric compounds had a considerable influence on the metabolic activity regarding COS-7 cells at the employed concentrations, which indicates again selectivity towards the ER-positive tumor cells.

3. Conclusion

Bivalent GW7604 and cyclofenilacrylic acid derivatives were synthesized to simultaneously target the ligand and the coactivator binding site within one ER monomer. By attaching at two sites within the ER LBD, the affinity to the ER should be strengthened and provide a mode of action different from well-known SERMs such as 4-OHT. This approach differs from the design of SERMs in order to optimize the effects of 4-OHT or GW7604 [44,45], respectively.

Based on the theoretical studies, it was obvious that the CABS can be addressed using Gln327 or Lys314 as H-bonding anchors. Other than that, hydrophobic contacts are suitable interactions at the ER surface for ligand binding as well. This part of the ER is easily accessible from the LBS using a C3, C4, or C5 spacer and a second drug molecule.

The most interesting compound, the cyclofenil derivative **15b**, displayed ER downregulatory potency of 38% at 1 μM (fulvestrant: 100%) and was able to displace E2 with an RBA = 79.2% from its binding site. It completely prevented the recruitment of the PGC1 coactivator peptide and abolished the E2-induced transactivation in U2OS cells, transiently transfected with the plasmids pSG5-ERα and the reporter plasmid p(ERE)2-luc^{+} with an IC_{50} = 68 nM.

All bivalent ER inhibitors were full antagonists without having agonistic side effects. In contrast to 4-OHT, they reduced the ERα content in MCF-7 cells, which was not prevented by the proteasome inhibitor MG-132. Therefore, they modulate the ER expression rather than the ER degradation. The cyclofenil-based homodimers seem to be slightly superior to the GW7604-based homodimers. However, this effect could be just obtained through the influence by the active isomers, as previously discussed.

The conformational change caused by simultaneously blocking both the LBS and the CABS is not clear yet, but it probably leads to an uncontrolled orientation of H12, prevention of AF2 formation and inhibition of coactivator binding. Introduction of a C3 spacer between two drug molecules appears to offer the best conditions for degradation. A complete destabilization as observed for fulvestrant is unlikely, because of the missing long side chain. A fulvestrant-like ER binding might impair receptor dimerization and energy-dependent nucleocytoplasmic shuttling, thereby blocking nuclear localization of the receptor [46,47].

Furthermore, the carboxylate of GW7604 is not essential for the ER downregulation. Additional contacts in the CABS upon derivation led to the same effects. The underlying drug design concept additionally enabled to prevent the stimulating effects observed by 4-OHT as well as by the use of cationic or uncharged side chains.

4. Experimental

4.1. Chemistry

4.1.1. Computational design of the homodimers

The 2D chemical structures were generated with ChemDraw (version 14.0.0.117). Energy minimization of the homodimers was performed using the MM2 force field calculation method of ChemBio3D Ultra [48]. GOLD suite 5.2 [49] was employed for the docking experiments. The binding site was defined in a 20 Å radius around the oxygen of Leu306 (atom coordinates 73.479, 8.386, 22.166). Other than that, default settings were used and no constraints were set. Ten binding postures per ligand were chosen and the results were examined in LigandScout 4.1 alpha4 [50]. Docking poses were evaluated visually and the GoldScore and the ChemPLP scoring function were compared, respectively. To ensure that there are no major differences in the binding mode to the LBS and the CABS of ERβ compared to those of ERα, the two crystal structures of ERα (3ERD [51]) and ERβ (3OLS [52]) were implemented and aligned using the program PyMol [53]. Prior to docking, the redocking of the two co-crystallized 4-OHT molecules was carried out for both the LBS and the CABS (root-mean-square deviation = 0.530 and 0.810, respectively).

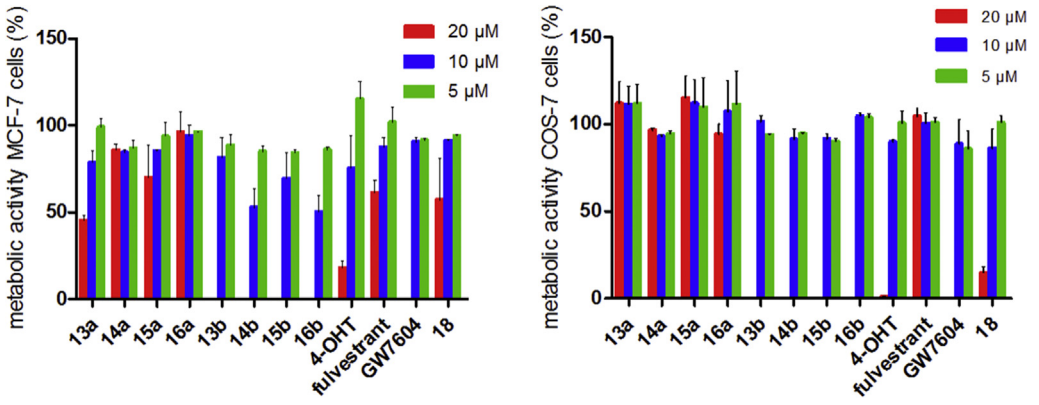

Fig. 10. Percentage metabolic activity compared to the DMSO control (set to 100%). The means + SD of ≥3 independent experiments is shown.

4.1.2. General

All reagents were purchased from Sigma-Aldrich, TCI, VWR, and Alfa Aesar and were used without further purification. All solvents were distilled before usage. Anhydrous solvents were obtained by distillation under argon over an appropriate drying agent. Anhydrous reactions were performed under an inert argon atmosphere using oven-dried glassware, septa and syringes. The reactions were monitored using thin-layer-chromatography (TLC) on Polygram® SIL G/UV_{254} silica gel polyester sheets (Macherey-Nagel, Düren, Germany), and visualized with UV light (254 or 366 nm). Chromatography purification on Silica gel 60 Å was performed employing either classic standard procedures or by using a Biotage Isolera 1 Flash purification system. ^{1}H and ^{13}C NMR spectra were obtained on a Varian Gemini-200 (now Agilent), 400 MHz Avance 4 Neo (Bruker), 600 MHz Avance II (Bruker) or 700 MHz Avance 4 Neo (Bruker) spectrometer. Deuterated chloroform ($CDCl_3$), dimethyl sulfoxide (DMSO-d_6), acetone ($(CD_3)_2CO$) and methanol (CD_3OD) were used as solvents for NMR. The chemical shifts in ppm were used as a reference to tetramethylsilane or the solvent peak. Coupling constants (*J*) are listed in Hertz (Hz). The purity of final compounds **13**–**16** as well as stability measurements based on compound **14a** were performed by using HPLC (Shimadzu) on a C18 column (Knauer) employing 10 μL injection volume, an acetonitrile-water gradient (flow rate 1.2 mL/min) with UV detection at 254 or 283 nm and 37 °C oven temperature. All final compounds were ≥95% pure (for HPLC spectra see Supplementary data). High resolution mass spectra were obtained from an Orbitrap Elite mass spectrometer (Thermo Fisher Scientific). Detailed experimental data for the preparation and characterization of compounds **8**–**12** are described in the Supplementary data.

4.1.3. Synthesis of the final compounds

If possible, the signals in the ^{1}H NMR spectra were assigned to the *EE*, *EZ*, or *ZZ* isomer or to their respective moieties (expressed as *E* and *Z* isomers). The proton proportions (with one decimal place) express the isomeric ratio. The signals in the ^{13}C NMR spectra were ascribed to the respective isomers based on **14a** and **15a** as representatives. The preparation of GW7604 (**12a**) and the cyclofenil derivative **12b** was performed according to known procedures and was further optimized (see Supplementary data).

4.1.3.1. General procedure for the preparation of homodimers with different spacer length. To a solution of **12a** or **12b** (2.1 eq) in anh. DMF (2 mL), PyBOP (2.2 eq) dissolved in anh. DCM (1 mL) was added at 0 °C under an argon atmosphere. The solution was stirred for 5 min, then DIPEA (4.0 eq) was added dropwise, followed by an aliquot of a freshly prepared stock solution of the respective diamine (1 eq) in anh. DMF (0.1–1 mL). After 30 min on ice, the mixture was allowed to warm to rt or was heated to 45 °C. The reaction was stopped after 20 h–72 h depending on the used diamine. Thereafter, the solvents were evaporated and the residue was dissolved in ethyl acetate and washed with 1N HCl. The aqueous layer was extracted twice with ethyl acetate. The combined organic layers were washed with brine and dried over anh. Na_2SO_4. Purification was achieved by two column chromatography runs first with DCM and MeOH (95:5 → 93:7) then ethyl acetate 100% as eluent affording the respective homodiamides [30,54–56].

*4.1.3.1.1. (E)-N,N'-(Ethane-1,2-diyl)bis[3-(4-((E/Z)-1-(4-hydroxyphenyl)-2-phenylbut-1-en-1-yl)phenyl)acrylamide] (**13a**).* **13a** was synthesized according to the general procedure described above: 100 mg of **12a** (0.27 mmol), 147 mg of PyBOP (0.28 mmol), 0.09 mL of DIPEA (0.51 mmol) and 7.7 mg of 1,2-diaminoethane (0.13 mmol) in 0.3 mL of anh. DMF. The solution was stirred at 45 °C for three days. **13a** was obtained as a yellowish, sparkling powder (29 mg, 0.040 mmol, 28%). Purity: 98.1%. ^{1}H NMR (700 MHz, DMSO-d_6, *EE:EZ:ZZ* = 25:50:25): δ 0.86 (t, ^{3}J = 7.3 Hz, 6H, CH_2CH_3), 2.39 (q, ^{3}J = 6.9 Hz, 2H, CH_2CH_3, *Z* isomers), 2.43 (q, ^{3}J = 7.4 Hz, 2H, CH_2CH_3, *E* isomers), 3.22 (s, 1H, $NHCH_2CH_2NH$, *EE* isomer), 3.27 (s, 2H, $NHCH_2CH_2NH$, *EZ* isomer), 3.32 (s, 1H, $NHCH_2CH_2NH$, *ZZ* isomer), 6.42 (d, ^{3}J = 8.5 Hz, 2H, Ar*H*, *Z* isomers), 6.45 (d, ^{3}J = 16.5 Hz, 1H, CHC*H*CON*H*, *E* isomers), 6.55–6.67 (m, 2H, Ar*H* + CHC*H*CONH, *Z* isomers), 6.77 (d, ^{3}J = 8.4 Hz, 2H, Ar*H*, *E* isomers), 6.80–6.84 (m, 2H, Ar*H*, *E* isomers), 7.00 (d, ^{3}J = 8.0 Hz, 2H, Ar*H*, *E* isomers), 7.03–7.25 (m, 14H, Ar*H*), 7.26 (d, ^{3}J = 15.4 Hz, 1H, C*H*CHCONH, *E* isomers), 7.41–7.50 (m, 1H, C*H*CHCONH, *Z* isomers), 7.50–7.62 (m, 2H, Ar*H*, *Z* isomers), 8.06–8.29 (m, 2H, N*H*), 9.21 (s, 1H, O*H*), 9.46 (s, 1H, O*H*). ^{13}C NMR (176 MHz, DMSO-d_6): δ 13.33, 13.38, 28.47, 28.61, 28.99, 38.55, 38.59, 38.60, 38.64, 114.45, 115.11, 121.60, 121.91, 126.15, 126.30, 126.66, 127.46, 127.90, 127.96, 129.35, 129.37, 129.61, 130.22, 130.81, 131.40, 132.19, 133.02, 133.23, 133.76, 137.87, 138.25, 138.27, 138.34, 138.36, 140.72, 141.67, 141.77, 141.84, 144.54, 144.68, 155.43, 156.29, 165.17, 165.20, 165.23. HRMS (*m*/*z*): calculated for $C_{52}H_{47}N_2O_4$ $[M-H]^-$: 763.3536, found: 763.3577.

*4.1.3.1.2. (E)-N,N'-(Propane-1,3-diyl)bis[3-(4-((E/Z)-1-(4-hydroxyphenyl)-2-phenylbut-1-en-1-yl)phenyl)acrylamide] (**14a**).* **14a** was synthesized according to the general procedure described above: 100 mg of **12a** (0.27 mmol), 147 mg of PyBOP (0.28 mmol), 0.062 mL of DIPEA (0.35 mmol) and 9.5 mg of 1,3-diaminopropane (0.13 mmol) in 1.0 mL of anh. DMF. The mixture was stirred at rt for 48 h. **14a** was obtained as a yellowish, sparkling powder (68 mg, 0.087 mmol, 63%). Purity: 98.8%. ^{1}H NMR (600 MHz, CD_3OD, *EE:EZ:ZZ* = 28:47:25): δ 0.92 (t, ^{3}J = 7.4 Hz, 6H, CH_2CH_3), 1.74 (p, ^{3}J = 6.8 Hz, 0.6H, $NHCH_2CH_2CH_2NH$, *EE* isomer), 1.78 (p, ^{3}J = 6.8 Hz, 0.9H, $NHCH_2CH_2CH_2NH$, *EZ* isomer), 1.83 (p, ^{3}J = 6.7 Hz, 0.5H, $NHCH_2CH_2CH_2NH$, *ZZ* isomer), 2.46 (2xq, 1.9H, ^{3}J = 7.3 Hz, CH_2CH_3, *Z* isomers), 2.51 (q, ^{3}J = 7.4 Hz, 2.1H, CH_2CH_3, *E* isomers), 3.35 (q, ^{3}J = 6.9 Hz, 2H, $NHCH_2CH_2CH_2NH$, *EZ* isomer), 3.39 (t, ^{3}J = 6.8 Hz, 1H, $NHCH_2CH_2CH_2NH$, *ZZ* isomer), 6.41 (d, ^{3}J = 7.9 Hz, 1.9H, Ar*H*, *Z* isomers), 6.42–6.47 (m, 1H, CHC*H*CONH, *E* isomers), 6.59 (d, ^{3}J = 15.8 Hz, 0.5H, CHC*H*CONH, *EZ* isomer), 6.61 (d, ^{3}J = 15.8 Hz, 0.5H, CHC*H*CONH, *ZZ* isomer), 6.64–6.68 (2xd, ^{3}J = 8.6 Hz, 1.9H, Ar*H*, *Z* isomers), 6.77 (d, ^{3}J = 7.8 Hz, 2.1H, Ar*H*, *E* isomers), 6.85–6.88 (2xd, ^{3}J = 8.3 Hz + 8.4 Hz, 2.1H, Ar*H*, *E* isomers), 7.03 (d, ^{3}J = 7.7 Hz, 2.1H, Ar*H*, *E* isomers), 7.08–7.18 (m, 12.1H, Ar*H*), 7.21–7.26 (2xd, ^{3}J = 8.2 Hz, 2H, Ar*H*, *Z* isomers), 7.34 (d, ^{3}J = 15.7 Hz, 0.5H, C*H*CHCONH, *EE* isomer), 7.35 (d, ^{3}J = 15.7 Hz, 0.5H, C*H*CHCONH, *EZ* isomer), 7.51–7.59 (m, 2.9H, Ar*H* + C*H*CHCONH). ^{13}C NMR (151 MHz, CD_3OD): δ 13.83 *E* isomers, 13.89 *Z* isomers, 29.88 *Z* isomers, 30.01 *E* isomers, 30.31–30.36, 38.03 EE isomer, 38.09 *EZ* isomer, 38.11 *EZ* isomer, 38.17 *ZZ* isomer, 115.28 *Z* isomers, 116.03 *E* isomers, 121.02 *E* isomers, 121.48 *Z* isomers, 127.22 *Z* isomers, 127.37 *E* isomers, 127.86 *E* isomers, 128.69 *Z* isomers, 128.94 *Z* isomers, 129.01 *E* isomers, 130.84 *Z* isomers, 130.86 *E* isomers, 131.12 *Z* isomers, 131.69 *E* isomers, 132.46 *E* isomers, 133.06 *Z* isomers, 133.54 *E* isomers, 134.62 *Z* isomers, 135.28 *Z* isomers, 135.59 *E* isomers, 139.54 *Z* isomers, 139.68 *E* isomers, 141.53, 142.84 *Z* isomers, 143.64 *E* isomers, 143.67 *Z* isomers, 143.91 *E* isomers, 146.80 *E* isomers, 147.05 *Z* isomers, 156.68 *Z* isomers, 157.57 *E* isomers, 168.87. HRMS (*m*/*z*): calculated for $C_{53}H_{51}N_2O_4$ $[M+H]^+$: 777.3771, found: 777.3742.

*4.1.3.1.3. (E)-N,N'-(Butane-1,4-diyl)bis[3-(4-((E/Z)-1-(4-hydroxyphenyl)-2-phenylbut-1-en-1-yl)phenyl)acrylamide] (**15a**).* **15a** was synthesized according to the general procedure described above: 78 mg of **12a** (0.21 mmol), 121 mg of PyBOP (0.23 mmol), 0.07 mL of DIPEA (0.42 mmol) and 8.9 mg of 1,4-diaminobutane (0.11 mmol) in 0.4 mL of anh. DMF were applied. The mixture was stirred at rt for 24 h. **15a** was obtained as yellowish, sparkling powder (31 mg, 0.039 mmol, 37%). Purity: 97.4%. ^{1}H NMR (700 MHz, CD_3OD, *EE:EZ:ZZ* = 29:49:22): δ 0.92 (3xt, 6H, 3x CH_2CH_3), 1.57–1.59 (m, 1.2H, $NHCH_2CH_2CH_2CH_2NH$, *EE* isomer), 1.61–1.63 (m,

2H, NHCH$_2$C*H*$_2$C*H*$_2$CH$_2$NH, *EZ* isomer), 1.65–1.67 (m, 0.9H, NHCH$_2$C*H*$_2$C*H*$_2$CH$_2$NH, *ZZ* isomer), 2.47 (q, ^3J = 7.4 Hz, 1.8H, C*H*$_2$CH$_3$, *Z* isomers), 2.52 (q, ^3J = 7.4 Hz, 2.2H, C*H*$_2$CH$_3$, *E* isomers), 3.29 (t, ^3J = 5.3 Hz 1.2H, NHC*H*$_2$CH$_2$CH$_2$C*H*$_2$NH, *EE* isomer), 3.33 (t, ^3J = 6.8 Hz, 2H, NHC*H*$_2$CH$_2$CH$_2$C*H*$_2$NH, *EZ* isomer), 3.36 (t, ^3J = 6.0 Hz, 0.9H, NHC*H*$_2$CH$_2$CH$_2$C*H*$_2$NH, *ZZ* isomer), 6.41–6.45 (m, 2.9H, Ar*H*, *Z* isomers + CHC*H*CONH, *E* isomers), 6.59 (d, ^3J = 15.8 Hz, 0.5H, CHC*H*CONH, *EZ* isomer), 6.61 (d, ^3J = 15.8 Hz, 0.4H, CHC*H*CONH, *ZZ* isomer), 6.66 (d, ^3J = 8.8 Hz, 1.9H, Ar*H*, *Z* isomers), 6.78 (2xd, 2.1H, Ar*H*, *E* isomers), 6.83–6.92 (2xd, ^3J = 8.3 Hz, 2.1H, Ar*H*, *E* isomers), 7.03 (d, ^3J = 8.7 Hz, 2.1H, Ar*H*, *E* isomers), 7.07–7.19 (m, 12.1H, Ar*H*), 7.21–7.27 (2xd, ^3J = 8.2 Hz, 1.9H, Ar*H*, *Z* isomers), 7.34 (d, ^3J = 15.7 Hz, 0.6H, C*H*CHCONH, *EE* isomer), 7.35 (d, ^3J = 15.8 Hz, 0.5H, C*H*CHCONH, *EZ* isomer), 7.49–7.57 (m, 2.8H, Ar*H* + C*H*CHCONH, *Z* isomers). ^{13}C NMR (176 MHz, CD$_3$OD): δ 13.82 *E* isomers, 13.87 *Z* isomers, 27.84 EE isomer, 27.89 *EZ* isomer, 27.93 *ZZ* isomer, 29.86 *Z* isomers, 30.00 *E* isomers, 40.16 EE isomer, 40.18 *EZ* isomer, 40.22 *EZ* isomer, 40.24 *ZZ* isomer, 115.28 *Z* isomers, 116.03 *E* isomers, 121.10 *E* isomers, 121.56 *Z* isomers, 127.22 *Z* isomers, 127.37 *E* isomers, 127.84 *E* isomers, 128.66 *Z* isomers, 128.93 *Z* isomers, 129.00 *E* isomers, 130.84 *Z* isomers, 130.86 *E* isomers, 131.11 *Z* isomers, 131.68 *E* isomers, 132.45 *E* isomers, 133.05 *Z* isomers, 133.58 *E* isomers, 134.66 *Z* isomers, 135.29 *Z* isomers, 135.61 *E* isomers, 139.55 *Z* isomers, 139.69 *E* isomers, 141.39 *E* isomers, 141.40 *Z* isomers, 142.84 *Z* isomers, 143.64 *E* isomers, 143.68 *Z* isomers, 143.90 *E* isomers, 146.75 *E* isomers, 147.01 *Z* isomers, 156.67 *Z* isomers, 157.57 *E* isomers, 168.76 *ZZ* isomer, 168.78 *EZ* isomer, 168.80 EE isomer. HRMS (*m*/*z*): calculated for $C_{54}H_{51}N_2O_4$ [M − H]$^-$: 791.3927, found: 791.3893.

*4.1.3.1.4. (E)-N,N'-(Pentane-1,5-diyl)bis[3-(4-((E/Z)-1-(4-hydroxyphenyl)-2-phenylbut-1-en-1-yl)phenyl)acrylamide] (**16a**).* **16a** was synthesized according to the general procedure described above: 50 mg of **12a** (0.14 mmol), 74 mg of PyBOP (0.23 mmol), 0.044 mL of DIPEA (0.26 mmol) and 6.6 mg of 1,5-diaminopentane (0.065 mmol) in 0.7 mL of anh. DMF. The mixture was stirred at rt for 48 h. **16a** was obtained as a yellowish, sparkling powder (17 mg, 0.021 mmol, 33.0%). Purity: 95.7%. ^{1}H NMR (600 MHz, CD$_3$OD, *EE:EZ:ZZ* = 29:49:22): δ 0.89–0.95 (3xt, 6H, 3x CH$_2$C*H*$_3$), 1.36–1.49 (m, 2H, NHCH$_2$CH$_2$C*H*$_2$CH$_2$CH$_2$NH), 1.53–1.67 (2xp, 4H, 2xNHCH$_2$C*H*$_2$CH$_2$C*H*$_2$CH$_2$NH), 2.47 (q, ^3J = 7.4 Hz, 1.9H, C*H*$_2$CH$_3$, *Z* isomers), 2.52 (2xq, ^3J = 7.4 Hz, 2.1H, 2xC*H*$_2$CH$_3$, *E* isomers), 3.25–3.35 (m, 4H, NHC*H*$_2$CH$_2$CH$_2$CH$_2$C*H*$_2$NH), 6.41–6.45 (m, 2.9H, Ar*H*, *Z* isomers + CHC*H*CONH, *E* isomers), 6.60 (d, ^3J = 15.8 Hz, 0.5H, CHC*H*CONH, *EZ* isomer), 6.62 (d, ^3J = 15.8 Hz, 0.4H, CHC*H*CONH, *ZZ* isomer), 6.66 (2xd, ^3J = 8.7 Hz, 1.9H, Ar*H*, *Z* isomers), 6.78 (2xd, ^3J = 8.5 Hz 2.1H, Ar*H*, *E* isomers), 6.86 (d, ^3J = 8.3 Hz, 2.1H, Ar*H*, *E* isomers), 7.03 (2xd, ^3J = 8.6 Hz, 2.1H, Ar*H*, *E* isomers), 7.06–7.19 (m, 12.1H, Ar*H*), 7.23 (d, ^3J = 8.2 Hz, 1.9H, Ar*H*, *Z* isomers), 7.34 (d, ^3J = 15.7 Hz, 0.6H, C*H*CHCONH, *EE* isomer), 7.35 (d, ^3J = 15.7 Hz, 0.5H, C*H*CHCONH, *EZ* isomer), 7.50–7.57 (m, 2.8H, Ar*H* + C*H*CHCONH, *Z* isomers). ^{13}C NMR (151 MHz, CD$_3$OD): δ 13.84, 13.90, 25.23, 29.89, 30.02, 30.04, 40.32, 40.38, 115.29, 116.04, 121.13, 121.60, 127.22, 127.37, 127.84, 128.66, 128.94, 129.01, 130.85, 130.87, 131.13, 131.69, 132.47, 133.07, 133.58, 134.67, 135.27, 135.58, 139.55, 139.69, 141.34, 142.83, 143.64, 143.68, 143.89, 146.74, 147.00, 156.70, 157.60, 168.77. HRMS (*m*/*z*): calculated for $C_{53}H_{51}N_2O_4$ [M − H]$^-$: 805.4084, found: 805.4050.

4.1.3.2. Cyclofenil-derived homodimers

*4.1.3.2.1. (E)-N,N'-(Ethane-1,2-diyl)bis[3-(4-(cyclohexylidene(4-hydroxyphenyl)methyl)phenyl)acrylamide] (**13b**).* **13b** was synthesized according to the general procedure described above: 56 mg of **12b** (0.17 mmol) in 0.5 mL of anh. DMF, 93 mg of PyBOP (0.18 mmol), 0.056 mL of DIPEA (0.32 mmol) and 4.9 mg of 1,2-diaminoethane (0.081 mmol) in 0.2 mL of anh. DMF. The mixture was stirred at rt for 24 h. Upon extraction, the organic phase was concentrated and the resulting precipitate filtered off and washed with MeOH and DCM. **13b** remained as a white powder (18 mg, 0.026 mmol, 32%). Purity: 95.4%. ^{1}H NMR (400 MHz, DMSO-d_6): δ 1.42–1.64 (m, 12H, C*H*$_2$), 2.07–2.25 (m, 8H, C*H*$_2$), 3.26–3.30 (m, 4H, C*H*$_2$), 6.56 (d, ^3J = 15.8 Hz, 2H, CHC*H*CONH), 6.68 (d, ^3J = 8.2 Hz, 4H, Ar*H*), 6.86 (d, ^3J = 8.2 Hz, 4H, Ar*H*), 7.08 (d, ^3J = 7.9 Hz, 4H, Ar*H*), 7.39 (d, ^3J = 15.7 Hz, 2H, CHC*H*CONH), 7.47 (d, ^3J = 7.9 Hz, 4H, Ar*H*), 8.21 (br, 2H, N*H*), 9.34 (br, 2H, O*H*). ^{13}C NMR (100 MHz, DMSO-d_6): δ 26.22, 28.16, 31.91, 31.95, 114.88, 121.59, 127.24, 129.96, 130.52, 132.67, 132.85, 133.55, 138.20, 138.48, 144.35, 155.85, 165.28. HRMS (*m*/*z*): calculated for $C_{46}H_{49}N_2O_4$ [M+H]$^+$: 693.3687, found: 693.3666.

*4.1.3.2.2. (E)-N,N'-(Propane-1,3-diyl)bis[3-(4-(cyclohexylidene(4-hydroxyphenyl)methyl)phenyl)acrylamide] (**14b**).* **14b** was synthesized according to the general procedure described above: 50 mg of **12b** (0.15 mmol) in 0.5 mL of anh. DMF, 83 mg of PyBOP (0.16 mmol), 0.05 mL of DIPEA (4 eq, 0.29 mmol) and 5.3 mg of 1,3-diaminopropane (0.072 mmol) in 0.3 mL of anh. DMF. The mixture was stirred for 24 h. After extraction and column chromatography purification with DCM and MeOH (98:2 → 95:5) followed by recrystallization from warm MeOH, **14b** was obtained as a white powder (34 mg, 0.048 mmol, 66%). Purity: 95.0%. ^{1}H NMR (400 MHz, DMSO-d_6): δ 1.41–1.61 (m, 12H, C*H*$_2$), 1.65 (p, ^3J = 6.5 Hz, 2H, NHCH$_2$C*H*$_2$CH$_2$NH), 2.08–2.25 (m, 8H, C*H*$_2$), 3.21 (q, ^3J = 6.6 Hz, 4H, NHC*H*$_2$CH$_2$C*H*$_2$NH), 6.57 (d, ^3J = 15.8 Hz, 2H, CHC*H*CONH), 6.68 (d, ^3J = 8.5 Hz, 4H, Ar*H*), 6.86 (d, ^3J = 8.5 Hz, 4H, Ar*H*), 7.08 (d, ^3J = 8.0 Hz, 4H, Ar*H*), 7.38 (d, ^3J = 15.7 Hz, 2H, C*H*CHCONH), 7.47 (d, ^3J = 8.0 Hz, 4H, Ar*H*), 8.12 (t, ^3J = 5.1 Hz, 2H, N*H*), 9.35 (br, 2H, O*H*). ^{13}C NMR (100 MHz, DMSO-d_6): δ 26.19, 28.13, 29.30, 31.89, 31.93, 36.65, 114.85, 121.67, 127.19, 129.92, 130.50, 132.71, 132.81, 133.54, 138.14, 138.27, 144.28, 155.83, 165.01. HRMS (*m*/*z*): calculated for $C_{47}H_{51}N_2O_4$ [M+H]$^+$: 707.3843, found: 707.3903.

*4.1.3.2.3. (E)-N,N'-(Butane-1,4-diyl)bis[3-(4-(cyclohexylidene(4-hydroxyphenyl)methyl)phenyl)acrylamide] (**15b**).* **15b** was synthesized according to the general procedure described above: 58 mg of **12b** (0.18 mmol) in 0.5 mL of anh. DMF, 96 mg of PyBOP (0.18 mmol), 0.06 mL of DIPEA (4 eq, 0.33 mmol) and 7.4 mg of 1,4-diaminobutane (0.084 mmol) in 0.5 mL of anh. DMF were stirred for 24 h. The next day, **15b** was filtered off by suction, washed with DCM and MeOH and remained as a white powder (45 mg, 0.064 mmol, 75%). Purity: 95.0%. ^{1}H NMR (400 MHz, DMSO-d_6): δ 1.37–1.49 (m, 4H, NHCH$_2$C*H*$_2$C*H*$_2$CH$_2$NH), 1.49–1.71 (m, 12H, C*H*$_2$), 2.01–2.82 (m, 8H, C*H*$_2$), 3.12–3.25 (m, 4H, NHC*H*$_2$CH$_2$CH$_2$C*H*$_2$NH), 6.56 (d, ^3J = 15.8 Hz, 2H, CHC*H*CONH), 6.68 (d, ^3J = 8.2 Hz, 4H, Ar*H*), 6.86 (d, ^3J = 8.1 Hz, 4H, Ar*H*), 7.08 (d, ^3J = 7.8 Hz, 4H, Ar*H*), 7.37 (d, ^3J = 15.7 Hz, 2H, CHC*H*CONH), 7.46 (d, ^3J = 7.8 Hz, 4H, Ar*H*), 8.08 (t, ^3J = 4.9 Hz, 2H, N*H*), 9.32 (s, 2H, O*H*). ^{13}C NMR (100 MHz, DMSO-d_6): δ 26.18, 26.72, 28.12, 31.87, 31.92, 38.39, 114.84, 121.76, 127.14, 129.90, 130.47, 132.73, 132.81, 133.54, 138.13, 144.22, 155.81, 164.88. HRMS (*m*/*z*): calculated for $C_{48}H_{53}N_2O_4$ [M+H]$^+$: 721.4000, found: 721.4090.

*4.1.3.2.4. (E)-N,N'-(Pentane-1,5-diyl)bis[3-(4-(cyclohexylidene(4-hydroxyphenyl)methyl)phenyl)acrylamide] (**16b**).* **16b** was synthesized according to the general procedure described above: 100 mg of **12b** (0.30 mmol) in 1 mL of anh. DMF, 165 mg of PyBOP (0.32 mmol), 0.10 mL of DIPEA (0.58 mmol) and 15 mg of 1,5-diaminopentane (0.08 mmol) in 0.7 mL of anh. DMF. The mixture was stirred for 24 h at rt. After extraction and concentration of the organic phase, the remaining solid was resuspended in DCM and filtered by vacuum suction. After washing carefully with DCM and cold MeOH, **16b** was isolated as a white powder (59 mg, 0.08 mmol, 56.2%), Purity: 95.2%. ^{1}H NMR (400 MHz, DMSO-d_6): δ 1.29–1.39 (m, 2H, NHCH$_2$CH$_2$C*H*$_2$CH$_2$CH$_2$NH), 1.44–1.61 (m, 16H, C*H*$_2$), 2.17 (bm, 8H, C*H*$_2$), 3.16 (bq, ^3J = 5.9 Hz, 4H, NHC*H*$_2$CH$_2$CH$_2$CH$_2$C*H*$_2$NH), 6.57

(d, ^3J = 15.8 Hz, 2H, CHC*H*CONH), 6.69 (d, ^3J = 8.4 Hz, 4H, Ar*H*), 6.86 (d, ^3J = 8.4 Hz, 4H, Ar*H*), 7.07 (d, ^3J = 8.0 Hz, 4H, Ar*H*), 7.37 (d, ^3J = 15.7 Hz, 2H, CHC*H*CONH), 7.45 (d, ^3J = 8.0 Hz, 4H, Ar*H*), 8.07 (bt, ^3J = 5.3 Hz, 2H, N*H*), 9.33 (s, 2H, O*H*). ^{13}C NMR (101 MHz, DMSO-d_6): δ 24.11, 26.46, 28.44, 28.95, 31.19, 32.23, 115.20, 121.87, 127.56, 130.22, 130.81, 132.94, 133.36, 133.25, 138.74, 138.63, 144.64, 156.00, 165.58. HRMS (*m*/*z*): calculated for $C_{49}H_{55}N_2O_4$ $[M+H]^+$: 735.4156, found: 735.4150.

*4.1.3.2.5. (E)-N-[2-(Boc-amino)ethyl]-3-[4-((E/Z)-1-(4-hydroxyphenyl)-2-phenylbut-1-enyl)phenyl]acrylamide (**17**).* **17** was synthesized according to the general procedure described above: 170 mg of **12a** (1.0 eq, 0.41 mmol), 213 mg of PyBOP (1.0 eq, 0.41 mmol), 0.28 mL of DIPEA (4.0 eq, 1.62 mmol) and 72 mg of *N*-Boc-1,2-diaminoethane (1.1 eq, 0.45 mmol) in 0.5 mL of anh. DMF. The solution was stirred for 24 h at rt. **17** was obtained as a white-yellow powder (105 mg, 0.20 mmol, 51%) [39,55–57]. ^{1}H NMR (200 MHz, CD_3OD, *E:Z* = 55:45): δ 0.93 (t, ^3J = 7.6 Hz, 3H, CH_2CH_3), 1.42 (s, 5H, OC(CH_3)$_3$, *E* isomer), 1.44 (s, 4H, OC(CH_3)$_3$, *Z* isomer), 2.42–2.58 (m, 2H, CH_2), 3.18–3.24 (m, 2H, CH_2), 3.35–3.42 (m, 2H, CH_2), 6.39–6.56 (m, 2H, CHC*H*CONH + Ar*H*), 6.66 (d, ^3J = 8.2 Hz, 0.9H, Ar*H*, *Z* isomer), 6.78 (d, ^3J = 8.4 Hz, 1.1H, Ar*H*, *E* isomer), 6.88 (d, ^3J = 8.2 Hz, 1.1H, Ar*H*, *E* isomer), 7.04 (d, ^3J = 8.6 Hz, 1.1H, Ar*H*, *E* isomer), 7.12–7.27 (m, 6.9H, Ar*H*), 7.36 (d, ^3J = 15.6 Hz, 0.6H, C*H*CHCONH, *E* isomer), 7.52–7.59 (m, 1.3H, C*H*CHCONH + Ar*H*, *Z* isomers).

*4.1.3.3. (E)-N-(2-Aminoethyl)-3-[4-((E/Z)-1-(4-hydroxyphenyl)-2-phenylbut-1-enyl)phenyl]acrylamide trifluoroacetate salt (**18**).* **18** was prepared using 105 mg of **17** (0.20 mmol) in 1.0 mL anh. DCM and 0.3 mL of TFA. The mixture was stirred under an argon atmosphere at 0 °C for 2 h, followed by the evaporation of the solvent under reduced pressure. The residue was treated with MeOH and DCM several times to remove remaining TFA and then evaporated to dryness yielding a brownish oil (107 mg, 0.20 mmol, quant.) [57]. ^{1}H NMR (200 MHz, CD_3OD, *E:Z* = 60:40): δ 0.92 (t, ^3J = 7.4 Hz, 3H, CH_2CH_3), 2.41–2.57 (m, 2H, CH_2CH_3), 3.06–3.16 (m, 2H, CH_2), 3.51–3.62 (m, 2H, CH_2), 6.40–6.68 (m, 3H, CHC*H*CONH + Ar*H*), 6.79 (d, ^3J = 8.6 Hz, 1.2H, Ar*H*, *E* isomer), 6.89 (d, ^3J = 8.2 Hz, 1.2H, Ar*H*, *E* isomer), 7.02–7.28 (m, 8.8H, Ar*H*, N*H*), 7.42 (d, ^3J = 16.0 Hz, 0.6H, C*H*CHCONH, *E* isomer), 7.55–7.65 (m, 1.2H, C*H*CHCONH + Ar*H*, *Z* isomer).

4.2. In vitro assays

4.2.1. General

The human osteosarcoma cell line U2OS, the human breast cancer cell lines MCF-7, MDA-MB-231, and SKBr-3 as well as the African green monkey kidney cell line COS-7 were obtained from the cell line service (CLS, Eppelheim, Germany). The cells were maintained as monolayer cultures. McCoy's 5A medium supplemented with 10% fetal bovine serum (FBS) (both from Biochrome GmbH, Berlin, Germany) was used for the U2OS and SKBr-3 cell lines and Dulbecco's modified eagle medium (DMEM) without phenol red, with glucose (4.5 g L^{-1}) (GE Healthcare, Pasching, Austria), supplemented with 10% FBS and 1% pyruvate (GE Healthcare) for MCF-7, MDA-MB-231, and COS-7 cell lines. They were cultivated in a humidified atmosphere (5% CO_2/95% air) at 37 °C and passaged twice a week. DMSO was used as a solvent for the investigated compounds. The final concentration of DMSO never exceeded 0.1% in cell based assays. Vehicle treated controls were always included.

4.2.2. Binding assays

LanthaScreen®TR-FRET ER alpha/beta Competitive Binding Assays (Invitrogen, Carlsbad, USA) were used according to the manufacturer's instructions to investigate the binding affinity to the LBD. The recombinant LBD of ERα/ERβ (4.2 nM), tagged with glutathione S-transferase (GST) was mixed with a terbium labeled anti-GST antibody (2 nM), Fluormone™ ES2 Green (3 nM) and 10 μL of a serial diluted stock solution of the compounds. Binding studies were performed in a concentration-dependent manner. TR-FRET was measured with an Enspire multimodal plate reader (PerkinElmer Life Sciences, Waltham, USA) using an excitation filter at 340/310 nm and emission filters for terbium at 495 nm and fluorescein at 520 nm. The TR-FRET ratio was calculated by dividing the emission signal of fluorescein by the emission signal of terbium.

The recruitment of coactivators was performed analogously with the LanthaScreen®TR-FRET ER alpha Coactivator Assay (Invitrogen, Carlsbad, USA). For the antagonistic mode the assay was performed with E2 4 nM.

4.2.3. Luciferase reporter gene assay

The transient transfection (TansIT-LT1, MoBiTec, Göttingen, Germany) and the dual-luciferase reporter assay (Promega, Madison, USA) were performed according to the manufacturer's protocols. U2OS cells were seeded in 96-well plates (1×10^4 cells per well) using McCoy's 5A medium supplemented with 10% charcoal dextran treated FBS as well as 1% penicillin/streptomycin and incubated at 37 °C in a humidified atmosphere (5% CO_2/95% air) for 24 h. Then, the cells were transiently transfected with pSG5-ERα (1 ng) or pSG5-ERβ (1 ng), respectively, p(ERE)2-luc$^+$ (50 ng) and pRenilla-CMV (0.5 ng) in phosphate-buffered saline (PBS) using TransIT®-LT1. After 6–8 h, the compounds were added in a concentration-dependent manner and incubated for 21 h, luciferase activity was measured employing an Enspire multimodal plate reader (PerkinElmer Life Sciences, Waltham, USA). Renilla luciferase activity was used as internal control and for normalization.

4.2.4. Cellular uptake

The cellular uptake was quantified by fluorimetry on an Enspire multimode plate reader and correlated to the protein content. MCF-7 cells (0.25×10^6 cells per well) or COS-7 (0.32×10^6 cells per well) were seeded (2 mL) in 6-well microtiter plates and kept at 37 °C in a humidified atmosphere (5% CO_2/95% air) for 24 h followed by further 24 h of drug incubation. The cells were rinsed with 2 mL of PBS and detached by adding 200 μL of accutase (GE Healthcare BioSciences, Pasching, Austria). Subsequently, the cells were harvested in 800 μL of PBS and the cell suspension was centrifuged (rt, 8000 rcf, 3 min). The supernatant was discarded, and the isolated cell pellets were washed with 1000 μL of PBS, resuspended, centrifuged and then stored at −20 °C for a maximum of two weeks until further analysis. After thawing, the cell pellets were resuspended in 300 μL of distilled water and lysed by sonification (setting parameter: 20 s, 9 cycles, 80–85% power). An aliquot was used for the Bradford protein assay to relate the amount of drug (nmol) to the protein content of the cell pellet (mg). The assay was performed according to a previously described method [58]. For fluorescence analysis, 100 μL of the lysates were diluted 1:1 with a mixture of distilled water and MeOH (9:1) in a black 96-well plate in duplicates. The excitation wavelength was set to 330 nm and the emission was measured at 463 nm on an Enspire multimodal plate reader (PerkinElmer Life Sciences, Waltham, USA). The average emission of duplicates was calculated. The values represent the means ± SD of ≥3 independent experiments.

4.2.5. Western blot

MCF-7 cells (0.5×10^6 cells per well) were seeded in 6-well plates in DMEM supplemented with 10% charcoal dextran treated FBS and 1% pyruvate. For adhesion, the cells were incubated for 24 h

overnight and then treated with 1 μM of compound dilutions for another 24 h. MG-132 (1 μM) was added half an hour before the compounds and it was incubated for 4 h. After treatment, cells were harvested and samples were lysed using a modified radio immunoprecipitation assay buffer (containing: 50 mM of Tris (pH = 8.0), 150 mM of NaCl, 0.5% NP-40, 50 mM of NaF, 1 mM of Na_3PO_4, 1 mM of phenylmethylsulfonyl fluoride (all from Sigma-Aldrich, Austria) and protease inhibitors (EDTA-free; Roche, Austria)). Total protein (30 μg) concentration was determined by using the Bradford assay (see above), then the proteins were processed by SDS-PAGE and transferred onto a nitrocellulose membrane (Amersham, GE Healthcare, Austria). Membranes were probed with ERα antibody (SP1, 1:1000, Invitrogen) and an HRP-labeled goat anti-rabbit (DAKO, Agilent, Austria) was used as a secondary reagent. Antibody specific β-actin (D6A8, 1:1000, Cell Signaling, Austria) confirmed equal loading of proteins. Detection was assessed by enhanced chemiluminescence (ECL, Thermo Scientific, Austria).

4.2.6. In-Cell Western immunoassay

Further investigations of the degradation were carried out using an In-Cell Western™ Assay Kit and the CellTag™ 700 Stain (LI-COR, Lincoln, USA). MCF-7 cells were seeded in 96-well plates (1×10^4 cells per well) in DMEM supplemented with 10% charcoal dextran treated FBS and 1% pyruvate. After 24 h, compounds were added and incubated for another 24 h at 37 °C in a humidified atmosphere (5% CO_2/95% air). Medium was aspirated, cells were fixed with a 3.7% formaldehyde solution and the assay was performed according to the manufacturer's instructions. ERα antibody (SP1, 1:250, Invitrogen) was used as primary antibody. Fluorescence intensity was recorded and quantified using the Odyssey Infrared Imaging System (LI-COR). DMSO and fulvestrant were used, respectively, to set the basis for maximum response and maximum efficacy of ERα downregulation.

4.2.7. Crystal violet assay

The antiproliferative and cytotoxicity evaluation was performed with the ER-positive MCF-7 cell line and the fibroblast-like cells COS-7 according to a modified protocol previously described [58]. Cells were seeded in 96-well microtiter plates (2×10^3 cells per well) in DMEM supplemented with 10% FBS and pyruvate. 24 h after seeding, the complete medium with the compounds was added in quadruples. After an incubation time of 72 h in a humidified atmosphere (5% CO_2/95% air) at 37 °C, the medium was aspirated, cells were washed with PBS (GE Healthcare) and fixed with a solution of 1% (v/v) glutaric dialdehyde in PBS. Cell biomass was determined *via* staining of the chromatin of adherent cells with crystal violet, extraction of the stain with ethanol (70% v/v) and subsequent measurement of the absorbance at 590 nm. Cell viability is expressed as percentage of cell viability of vehicle-treated control which was set at 100%. Results are the means ± SD of ≥3 independent experiments.

4.2.8. EZ4U assay

Metabolic activity was evaluated analogously to the antiproliferative potency as described above. After 72 h of incubation, the metabolic activity was investigated employing a modified MTT assay (EZ4U Kit, Biomedica, Vienna, Austria) according to the manufacturer's protocol. The final data represent the means ± SD of ≥3 independent experiments.

Declaration of competing interest

The authors declare that they have no known competing financial interest or personal relationships that could have appeared to influence the work reported in this paper.

CRediT authorship contribution statement

Alexandra Knox: Conceptualization, Data curation, Formal analysis, Investigation, Methodology, Writing - original draft, Writing - review & editing. **Christina Kalchschmid:** Data curation, Formal analysis, Investigation, Methodology, Writing - original draft, Writing - review & editing. **Daniela Schuster:** Resources, Software, Investigation. **Francesca Gaggia:** Investigation. **Claudia Manzl:** Resources, Investigation. **Daniel Baecker:** Investigation, Writing - review & editing. **Ronald Gust:** Conceptualization, Supervision, Writing - review & editing.

Acknowledgements

We thank Christoph Kreutz (Institute of Organic Chemistry, University of Innsbruck) and Peter Schneider (Institute of Pharmacy, Department of Pharmacognosy, University of Innsbruck) for recording the ^1H and ^{13}C NMR spectra and André Betz (Institute of Pharmacy, Department of Pharmaceutical Chemistry, University of Innsbruck) for assistance in the crystal violet assay. We also thank Inte:Ligand GmbH for providing an academic license of LigandScout. The Austrian Research Promotion Agency FFG [West Austrian BioNMR 858017] is also kindly acknowledged.

Appendix B. Supplementary data

Supplementary data to this article can be found online at https://doi.org/10.1016/j.ejmech.2020.112191.

Appendix A. Supplementary data

Supplementary data associated with this article is available free of charge in the online version.

References

[1] V.C. Jordan, Antiestrogens and selective estrogen receptor modulators as multifunctional medicines. 1. Receptor interactions, J. Med. Chem. 46 (2003) 883–908.
[2] V.C. Jordan, Antiestrogens and selective estrogen receptor modulators as multifunctional medicines. 2. Clinical considerations and new agents, J. Med. Chem. 46 (2003) 1081–1111.
[3] A.L. Rodriguez, A. Tamrazi, M.L. Collins, J.A. Katzenellenbogen, Design, synthesis, and in vitro biological evaluation of small molecule inhibitors of estrogen receptor alpha coactivator binding, J. Med. Chem. 47 (2004) 600–611.
[4] A. Sun, T.W. Moore, J.R. Gunther, M.S. Kim, E. Rhoden, Y. Du, H. Fu, J.P. Snyder, J.A. Katzenellenbogen, Discovering small-molecule estrogen receptor alpha/coactivator binding inhibitors: high-throughput screening, ligand development, and models for enhanced potency, ChemMedChem 6 (2011) 654–666.
[5] W. Qin, M. Xie, X. Qin, Q. Fang, F. Yin, Z. Li, Recent advances in peptidomimetics antagonists targeting estrogen receptor alpha-coactivator interaction in cancer therapy, Bioorg. Med. Chem. Lett. 28 (2018) 2827–2836.
[6] K.E. Bergmann, C.H. Wooge, K.E. Carlson, B.S. Katzenellenbogen, J.A. Katzenellenbogen, Bivalent ligands as probes of estrogen receptor action, J. Steroid Biochem. Mol. Biol. 49 (1994) 139–152.
[7] A.L. LaFrate, K.E. Carlson, J.A. Katzenellenbogen, Steroidal bivalent ligands for the estrogen receptor: design, synthesis, characterization and binding affinities, Bioorg. Med. Chem. 17 (2009) 3528–3535.
[8] A.E. Wendlandt, S.M. Yelton, D. Lou, D.S. Watt, D.J. Noonan, Synthesis and functional analysis of novel bivalent estrogens, Steroids 75 (2010) 825–833.
[9] M. Shan, A. Bujotzek, F. Abendroth, A. Wellner, R. Gust, O. Seitz, M. Weber, R. Haag, Conformational analysis of bivalent estrogen receptor ligands: from intramolecular to intermolecular binding, ChemBioChem 12 (2011) 2587–2598.
[10] M. Shan, K.E. Carlson, A. Bujotzek, A. Wellner, R. Gust, M. Weber, J.A. Katzenellenbogen, R. Haag, Nonsteroidal bivalent estrogen ligands: an application of the bivalent concept to the estrogen receptor, ACS Chem. Biol. 8 (2013) 707–715.
[11] Y. Wang, N.Y. Chirgadze, S.L. Briggs, S. Khan, E.V. Jensen, T.P. Burris, A second binding site for hydroxytamoxifen within the coactivator-binding groove of estrogen receptor beta, Proc. Natl. Acad. Sci. U.S.A. 103 (2006) 9908–9911.
[12] D.J. Kojetin, T.P. Burris, E.V. Jensen, S.A. Khan, Implications of the binding of tamoxifen to the coactivator recognition site of the estrogen receptor, Endocr. Relat. Cancer 15 (2008) 851–870.

[13] A.C.W. Pike, A.M. Brzozowski, J. Walton, R.E. Hubbard, A.G. Thorsell, Y.L. Li, J.Å. Gustafsson, M. Carlquist, Structural insights into the mode of action of a pure antiestrogen, Structure 9 (2001) 145–153.

[14] B.M. Wittmann, A. Sherk, D.P. McDonnell, Definition of functionally important mechanistic differences among selective estrogen receptor down-regulators, Canc. Res. 67 (2007) 9549–9560.

[15] A. Lai, M. Kahraman, S. Govek, J. Nagasawa, C. Bonnefous, J. Julien, K. Douglas, J. Sensintaffar, N. Lu, K.J. Lee, A. Aparicio, J. Kaufman, J. Qian, G. Shao, R. Prudente, M.J. Moon, J.D. Joseph, B. Darimont, D. Brigham, K. Grillot, R. Heyman, P.J. Rix, J.H. Hager, N.D. Smith, Identification of GDC-0810 (ARN-810), an orally bioavailable selective estrogen receptor degrader (SERD) that demonstrates robust activity in tamoxifen-resistant breast cancer xenografts, J. Med. Chem. 58 (2015) 4888–4904.

[16] C. De Savi, R.H. Bradbury, A.A. Rabow, R.A. Norman, C. de Almeida, D.M. Andrews, P. Ballard, D. Buttar, R.J. Callis, G.S. Currie, J.O. Curwen, C.D. Davies, C.S. Donald, L.J.L. Feron, H. Gingell, S.C. Glossop, B.R. Hayter, S. Hussain, G. Karoutchi, S.G. Lamont, P. MacFaul, T.A. Moss, S.E. Pearson, M. Tonge, G.E. Walker, H.M. Weir, Z. Wilson, Optimization of a novel binding motif to (E)-3-(3,5-difluoro-4-((1R,3R)-2-(2-fluoro-2-methylpropyl)-3-methyl-2,3,4,9-tetrahydro-1H-pyrido[3,4-b]indol-1-yl)phenyl)acrylic acid (AZD9496), a potent and orally bioavailable selective estrogen receptor downregulator and antagonist, J. Med. Chem. 58 (2015) 8128–8140.

[17] G.S. Tria, T. Abrams, J. Baird, H.E. Burks, B. Firestone, L.A. Gaither, L.G. Hamann, G. He, C.A. Kirby, S. Kim, F. Lombardo, K.J. Macchi, D.P. McDonnell, Y. Mishina, J.D. Norris, J. Nunez, C. Springer, Y. Sun, N.M. Thomsen, C. Wang, J. Wang, B. Yu, C.L. Tiong-Yip, S. Peukert, Discovery of LSZ102, a potent, orally bioavailable selective estrogen receptor degrader (SERD) for the treatment of estrogen receptor positive breast cancer, J. Med. Chem. 61 (2018) 2837–2864.

[18] Y.L. Wu, X. Yang, Z. Ren, D.P. McDonnell, J.D. Norris, T.M. Willson, G.L. Greene, Structural basis for an unexpected mode of SERM-mediated ER antagonism, Mol. Cell 18 (2005) 413–424.

[19] T.M. Willson, B.R. Henke, T.M. Momtahen, P.S. Charifson, K.W. Batchelor, D.B. Lubahn, L.B. Moore, B.B. Oliver, H.R. Sauls, J.A. Triantafillou, S.G. Wolfe, P.G. Baer, 3-[4-(1,2-Diphenylbut-1-enyl)phenyl]acrylic acid: a non-steroidal estrogen with functional selectivity for bone over uterus in rats, J. Med. Chem. 37 (1994) 1550–1552.

[20] D. Bentrem, R. Dardes, H. Liu, J. MacGregor-Schafer, J. Zapf, V.C. Jordan, Molecular mechanism of action at estrogen receptor alpha of a new clinically relevant antiestrogen (GW7604) related to tamoxifen, J. Endocrinol. 142 (2001) 838–846.

[21] S.W. Fanning, L. Hodges-Gallagher, D.C. Myles, R. Sun, C.E. Fowler, I.N. Plant, B.D. Green, C.L. Harmon, G.L. Greene, P.J. Kushner, Specific stereochemistry of OP-1074 disrupts estrogen receptor alpha helix 12 and confers pure antiestrogenic activity, Nat. Commun. 9 (2018) 2368.

[22] K.J. Kieser, D.W. Kim, K.E. Carlson, B.S. Katzenellenbogen, J.A. Katzenellenbogen, Characterization of the pharmacophore properties of novel selective estrogen receptor downregulators (SERDs), J. Med. Chem. 53 (2010) 3320–3329.

[23] J. Min, V.S. Guillen, A. Sharma, Y. Zhao, Y. Ziegler, P. Gong, C.G. Mayne, S. Srinivasan, S.H. Kim, K.E. Carlson, K.W. Nettles, B.S. Katzenellenbogen, J.A. Katzenellenbogen, Adamantyl antiestrogens with novel side chains reveal a spectrum of activities in suppressing estrogen receptor mediated activities in breast cancer cells, J. Med. Chem. 60 (2017) 6321–6336.

[24] I. Paterni, C. Granchi, J.A. Katzenellenbogen, F. Minutolo, Estrogen receptors alpha (ERα) and beta (ERβ): subtype-selective ligands and clinical potential, Steroids 90 (2014) 13–29.

[25] M.J. Li, H.M. Greenblatt, O. Dym, S. Albeck, A. Pais, C. Gunanathan, D. Milstein, H. Degani, J.L. Sussman, Structure of estradiol metal chelate and estrogen receptor complex: the basis for designing a new class of selective estrogen receptor modulators, J. Med. Chem. 54 (2011) 3575–3580.

[26] J.F. Eaddy, D. Heyer, S.R. Katamreddy, M.T. Martin, M.S. McClure, A.S. Randhawa, V. Samano, J.A. Ray, Preparation of acyloxydiphenylbutenylcinnamates as estrogen receptor modulator prodrugs, 2005. WO2005/033056A2.

[27] J.F. Eaddy, D. Heyer, S.R. Katamreddy, M.T. Martin, M.S. MCClure, A.S. Randhawa, V. Samano, J.A. Ray, Triphenylethylene compounds as selective estrogen receptor modulators, 2008. EP1692127A2.

[28] M. Fan, E.L. Rickert, L. Chen, S.A. Aftab, K.P. Nephew, R.V. Weatherman, Characterization of molecular and structural determinants of selective estrogen receptor downregulators, Breast Cancer Res. Treat. 103 (2007) 37–44.

[29] V. Lubczyk, H. Bachmann, R. Gust, Investigations on estrogen receptor binding. The estrogenic, antiestrogenic, and cytotoxic properties of C2-alkyl-substituted 1,1-bis(4-hydroxyphenyl)-2-phenylethenes, J. Med. Chem. 45 (2002) 5358–5364.

[30] J. Coste, D. Le-Nguyen, B. Castro, PyBOP®: a new peptide coupling reagent devoid of toxic by-product, Tetrahedron Lett. 31 (1990) 205–208.

[31] V.W. Winkler, M.A. Nyman, R.S. Egan, Diethylstilbestrol cis-trans isomerization and estrogen activity of diethylstilbestrol isomers, Steroids 17 (1971) 197–207.

[32] J.A. Katzenellenbogen, K.E. Carlson, B.S. Katzenellenbogen, Facile geometric isomerization of phenolic non-steroidal estrogens and antiestrogens: limitations to the interpretation of experiments characterizing the activity of individual isomers, J. Steroid Biochem. 22 (1985) 589–596.

[33] C. Malet, P. Spritzer, C. Cumins, D. Guillaumin, P. Mauvais-Jarvis, F. Kuttenn, Effect of 4-hydroxytamoxifen isomers on growth and ultrastructural aspects of normal human breast epithelial (HBE) cells in culture, J. Steroid Biochem. Mol. Biol. 82 (2002) 289–296.

[34] D.C. Hilt, V. Masini-Eteve, R. Fedynec, B. Taravella, Chemically stable compositions of 4-hydroxytamoxifen, 2005. WO 2005/092310.

[35] R.V. Weatherman, N.J. Clegg, T.S. Scanlan, Differential SERM activation of the estrogen receptors (ERα and ERβ) at AP-1 sites, Chem. Biol. 8 (2001) 427–436.

[36] V.C. Jordan, M.M. Collins, L. Rowsby, G. Prestwich, A monohydroxylated metabolite of tamoxifen with potent antioestrogenic activity, J. Endocrinol. 75 (1977) 305–316.

[37] K.E. Allen, E.R. Clark, V.C. Jordan, Evidence for the metabolic activation of non-steroidal antioestrogens: a study of structure-activity relationships, Br. J. Pharmacol. 71 (1980) 83–91.

[38] Z. Nawaz, D.M. Lonard, A.P. Dennis, C.L. Smith, B.W. O'Malley, Proteasome-dependent degradation of the human estrogen receptor, Proc. Natl. Acad. Sci. U.S.A. 96 (1999) 1858–1862.

[39] I. Laios, F. Journe, D. Nonclercq, D.S. Vidal, R.A. Toillon, G. Laurent, G. Leclercq, Role of the proteasome in the regulation of estrogen receptor alpha turnover and function in MCF-7 breast carcinoma cells, J. Steroid Biochem. Mol. Biol. 94 (2005) 347–359.

[40] H. Reile, H. Birnböck, G. Bernhardt, T. Spruß, H. Schönenberger, Computerized determination of growth kinetic curves and doubling times from cells in microculture, Anal. Biochem. 187 (1990) 262–267.

[41] J. Liu, S. Zheng, S. Guo, C. Zhang, Q. Zhong, Q. Zhang, P. Ma, E.V. Skripnikova, M.R. Bratton, T.E. Wiese, G. Wang, Rational design of a boron-modified triphenylethylene (GLL398) as an oral selective estrogen receptor down-regulator, ACS Med. Chem. Lett. 8 (2017) 102–106.

[42] I.N. White, F. de Matteis, A. Davies, L.L. Smith, C. Crofton-Sleigh, S. Venitt, A. Hewer, D.H. Phillips, Genotoxic potential of tamoxifen and analogues in female Fischer F344/n rats, DBA/2 and C57BL/6 mice and in human MCL-5 cells, Carcinogenesis 13 (1992) 2197–2203.

[43] K. Niwa, S. Morishita, M. Hashimoto, T. Itoh, J. Fujimoto, H. Mori, T. Tamaya, Effects of tamoxifen on endometrial carcinogenesis in mice, Jpn. J. Cancer Res. 89 (1998) 502–509.

[44] B. Abderrahman, V.C. Jordan, Improving long-term adjuvant anti-oestrogenic therapy for breast cancer, Clin. Pharm. 8 (2016), https://doi.org/10.1211/CP.2016.20201203.

[45] B. Abderrahman, V.C. Jordan, Successful targeted therapies for breast cancer: the worcester foundation and future opportunities in women's health, Endocrinology 159 (2018) 2980–2990.

[46] S.E. Fawell, R. White, S. Hoare, M. Sydenham, M. Page, M.G. Parker, Inhibition of estrogen receptor-DNA binding by the "pure" antiestrogen ICI 164,384 appears to be mediated by impaired receptor dimerization, Proc. Natl. Acad. Sci. U.S.A. 87 (1990) 6883–6887.

[47] S. Dauvois, R. White, M.G. Parker, The antiestrogen ICI 182780 disrupts estrogen receptor nucleocytoplasmic shuttling, J. Cell Sci. 106 (1993) 1377–1388.

[48] PerkinElmer Informatics ®. 1998-2014.

[49] G. Jones, P. Willett, R.C. Glen, A.R. Leach, R. Taylor, Development and validation of a genetic algorithm for flexible docking, J. Mol. Biol. 267 (1997) 727–748.

[50] G. Wolber, T. Langer, LigandScout: 3-D pharmacophores derived from protein-bound ligands and their use as virtual screening filters, J. Chem. Inf. Model. 45 (2005) 160–169.

[51] A.K. Shiau, D. Barstad, P.M. Loria, L. Cheng, P.J. Kushner, D.A. Agard, G.L. Greene, The structural basis of estrogen receptor/coactivator recognition and the antagonism of this interaction by tamoxifen, Cell 95 (1998) 927–937.

[52] S. Möcklinghoff, R. Rose, M. Carraz, A. Visser, C. Ottmann, L. Brunsveld, Synthesis and crystal structure of a phosphorylated estrogen receptor ligand binding domain, ChemBioChem 11 (2010) 2251–2254.

[53] L.L.C. Schrödinger, The PyMOL Molecular Graphics System, 2006. Version 0.99.

[54] L.H. Lin, L.W. Lee, S.Y. Sheu, P.Y. Lin, Study on the stevioside analogues of steviolbioside, steviol, and isosteviol 19-alkyl amide dimers: synthesis and cytotoxic and antibacterial activity, Chem. Pharm. Bull. 52 (2004) 1117–1122.

[55] E. Rivero-Buceta, P. Carrero, E.G. Doyagüez, A. Madrona, E. Quesada, M.J. Camarasa, M.J. Peréz-Pérez, P. Leyssen, J. Paeshuyse, J. Balzarini, J. Neyts, A. San-Félix, Linear and branched alkyl-esters and amides of gallic acid and other (mono-, di- and tri-) hydroxy benzoyl derivatives as promising anti-HCV inhibitors, Eur. J. Med. Chem. 92 (2015) 656–671.

[56] M. Shan, Design, synthesis, and evaluation of bivalent estrogen ligands, Freie Universität Berlin, Berlin, 2011. PhD Thesis.

[57] C.B. Vu, J.E. Bemis, M.R. Jirousek, J.C. Milne, J.J. Smith, Preparation of fatty acid acylated salicylates for the treatment of inflammatory disorders, 2010. US2010/0184730A1.

[58] V. Obermoser, D. Baecker, C. Schuster, V. Braun, B. Kircher, R. Gust, Chlorinated cobalt alkyne complexes derived from acetylsalicylic acid as new specific antitumor agents, Dalton Trans. 47 (2018) 4341–4351.